

REPLICATION OF FREEFORM OPTICS ONTO NEAR-NET-SHAPE SUBSTRATES  
USING DIAMOND TURNED STAMPERS

by

Glen D. Smith

A thesis submitted to the faculty of  
The University of North Carolina at Charlotte  
in partial fulfillment of the requirements  
for the degree of Master of Science in  
Mechanical Engineering

Charlotte

2019

Approved by:

---

Dr. Matthew A. Davies

---

Dr. Joseph D. Owen

---

Dr. Thomas J. Suleski

---

Dr. Christopher J. Evans



## ABSTRACT

GLEN D. SMITH. Replication of freeform optics onto substrates using diamond turned polymer stampers. (Under the direction of DR. MATTHEW A. DAVIES)

Freeform optics open a new design space for optical systems. Production of freeform optics, with no axis of rotational symmetry, often requires the use of multi-axis (>2) sub aperture machining and finishing techniques. These are expensive and impede the widespread use of freeform optics. Thus, high-volume manufacturing techniques such as injection molding and precision glass molding are needed. This thesis investigates a hybrid replication technique in which a freeform corrective surface is replicated into a near-net-shape glass substrate. Because many freeform optical designs utilize optics that are nearly spherical, in this work we use an ultraviolet (UV) curable polymer to produce a freeform surface on inexpensive spherical UV transparent substrates. The process in this research proceeds as follows. A UV polymer is applied to the substrate. A freeform stamper is brought into contact with the substrate to shape the polymer. The polymer is cured by UV exposure and the stamper is removed. This work involved numerous diverse research challenges: (1) the choice of a suitable UV curable polymer and stamper combination using adhesion chemistry and empirical testing; (2) alignment of the stamper and the substrate in a UV curing chamber; (3) production and testing of a replication system including a freeform stamper; (4) testing of the replication process and associated metrology; (5) correction for shrinkage of the UV polymer during the curing process. Research indicates that the process is viable for producing near spherical freeforms with less than 1 micrometer of figure error. However, the only

stamper material that repeatedly releases from the optical surface formed by the UV curable polymer has been bulk polytetrafluoroethylene (PTFE, i.e. Teflon). The cutting mechanics of this material lead to a poor surface finish on the stamper (70 nm – 100 nm Sq) and this limits the surface roughness of the replicated optical surface. Future work is required to solve this problem, possibly with diamond turnable nickel plating containing polytetrafluoroethylene.

## DEDICATION

I would like to dedicate this work to my family who have supported me through my time at UNCC and always encourage, love, and uplift me. Thank you from the bottom of my heart.

## ACKNOWLEDGMENTS

I would like to acknowledge and thank Dr. Matthew A. Davies for advising me during this project. I would not be as passionate about learning if it were not for his enthusiasm and excellent teaching. Thank you for supporting me in my work and helping me to better understand how to learn. I would also like to thank Dr. Joseph D. Owen for his time and expertise. Dr. Owen spent countless hours helping me machine parts and better understand how to utilize the diamond turning machine. He was first my instructor when I was a sophomore and taught me how to use the manual mill and lathe and has continued to instruct me on the diamond turning machine. I would also like to thank Dr. Thomas J. Suleski and Christopher J. Evans for their wisdom and insight. Thank you both for the guidance and suggestions when I come knocking.

I would also like to thank everyone in the Freeform Optics Research Group for their help and encouragement. I would like to thank Dustin Gurganus for helping me transition into this project and into graduate life. I would like to thank Nick Horvath for the guidance and knowledge in the machine shop and on the bike trail. I would like to thank Nicholas Sizemore for his help doing the cutting experiments. I appreciate all the times that you have done measurements for the project. Thank you for suggesting good Thai food. I would also like to thank Prithiviraj Shanmugam (Raj) for his help and wisdom when taking measurements. Thank you for helping me to understand my measurements and sending me good papers to read. I would also like to thank all of you for helping specifically with CeFO-11. Thank you all for your friendships, I could not have asked for a better research group.

Lastly, I would like to thank The Center for Freeform Optics and all the project supporters for funding this project.

## TABLE OF CONTENTS

LIST OF TABLES .....	x
LIST OF FIGURES .....	xi
PREFACE .....	xiv
CHAPTER 1: BACKGROUND AND MOTIVATION.....	1
1.1 Importance of Freeform Optics.....	1
1.2 Precision Glass Molding .....	3
1.3 Replication of Optics and Micro-Optics .....	4
1.4 Conceptual Approach to Freeform Replication on a Near-net-shape Substrate .....	6
1.5 Adhesion Mechanics.....	8
1.6 Teflon Turning Mechanics.....	10
CHAPTER 2: KINEMATICS OF REPLICATION .....	13
2.1 Introduction.....	13
2.2 Experimental Setup.....	13
2.2.1 Background .....	13
2.2.2 Automated Replication System.....	18
2.2.3 Triangular Kinematic Replication System.....	20
2.2.4 Replication System with Spacer Ring.....	25
2.2.5 Replication System with Split Spacer .....	29
CHAPTER 3: DYNAMICS OF REPLICATION .....	33

3.1 Introduction.....	33
3.2 Equipment Used.....	35
3.3 Experimental Set Up.....	39
3.3.1 Sputtered Gold .....	42
3.4 Measurement Analysis and Results .....	45
CHAPTER 4: SURFACE ROUGHNESS OF DIAMOND TURNED TEFLON .....	50
4.1 Introduction.....	50
4.2 Experimental Setup.....	51
4.3 Results and Discussion .....	58
4.4 Conclusions and Future Work .....	66
CHAPTER 5: REPLICATION RESULTS.....	68
5.1 Introduction.....	68
5.2 Equipment Used.....	70
5.3 Shrinkage analysis using ‘top hat’ geometry .....	70
5.4 Spherical Replications .....	74
5.5 Shrinkage Correction .....	76
CHAPTER 6: CONCLUSIONS AND FUTURE WORK.....	81
6.1 Introduction.....	81
REFERENCES .....	82

## LIST OF TABLES

TABLE 1: Feed rates and RPM for the two chosen cutting velocities.....	52
TABLE 2 Values generated using the processing statistics function of Mx .....	57
TABLE 3 Spatial wavelength from the PSD for the three data sets .....	62

## LIST OF FIGURES

FIGURE 1.1 Original concept .....	7
FIGURE 2.1 Copper, brass, and aluminum stampers with sinewave .....	15
FIGURE 2.2 Replication process showing (a) aluminum stamper with a controlled sinusoidal feature; (b) glass slide on rim of stamper with polymer fill prior to curing; and (c) fully cured polymer on glass slide with some visible edge defects. ....	16
FIGURE 2.3 (a) Sample scanning white light interferometer measurement of the stamper; (b) Sample scanning white light interferometer measurement of replica; and (c) mean and standard deviation of PV amplitude measurements of sine wave on stamper and two replicas. ....	18
FIGURE 2.4 Replication system using kinematics alignment and stepper motor drives. ....	19
FIGURE 2.5 Kinematic replication system with spherical aluminum stamper (right) and glass substrate (left). ....	20
FIGURE 2.6 (a) Plot of stamper and substrate base radius (b) shows the gap as a function of radial position $r$ (mm). ....	22
FIGURE 2.7 Kelvin Clamp model.....	23
FIGURE 2.8 Three optic demonstrator with increased focal length/decreased power (left) original lens substrate (center) and decreased focal length/increased power (right) .....	25
FIGURE 2.9 New replication system using spacer ring comprising substrate holder a.) spacer ring b.) and stamper c.) .....	26
FIGURE 2.10 Cross-sectional view of the replications system showing stamper (red), spacer (blue), and substrate holder (green) .....	27
FIGURE 2.11 Substrate holder CAD a.) model and finished part b.) .....	28
FIGURE 2.12 Three-piece spacer and gold coated Aluminum stamper .....	29
FIGURE 2.13 Split ring replication system assembly showing a.) Teflon stamper b.) spacer ring c.) substrate holder .....	30
FIGURE 2.14 Split spacer ring CAD a.) and finished part b.) .....	31

FIGURE 2.15 Substrate holder with mounting features CAD a.) and finished part b.) ...	32
FIGURE 3.1 Kistler 3-axis dynamometer 9256C1 (left) and the charge amplifier (right)	35
FIGURE 3.2 National Instruments USB-6251 DAQ board.....	36
FIGURE 3.3 Arduino Uno with Adafruit motor shield .....	37
FIGURE 3.4 Geared DC motor and aluminum motor mount.....	38
FIGURE 3.5 Eccentric cam actuator on DC moto.....	38
FIGURE 3.6 The ELC-500 Light Exposure System by Electro-Lite Corporation.....	39
FIGURE 3.7 Force measurement set up .....	40
FIGURE 3.8 PMMA puck with masked areas for slides.....	41
FIGURE 3.9 Aluminum flat sputtered with 50nm of gold .....	43
FIGURE 3.10 Replicated flat with 50nm of Gold .....	44
FIGURE 3.11 Aluminum flat sputtered with 25nm of Gold .....	45
FIGURE 3.14 Force measurement from PMMA with and without partial release .....	46
FIGURE 3.15 Force measurements for Teflon at different cure times.....	47
FIGURE 3.16 Maximum force from measurements of Teflon, aluminum, and PMMA .	48
FIGURE 4.1 (a.) Teflon sample (b.) cross section showing 9 different 0.5 mm radial bands between the arrows .....	53
FIGURE 4.2 Diamond turned surface profile modeled as elliptical arcs .....	55
FIGURE 4.3 Areal data with 10 profiles used to calculate the average Ra of the surface	56
FIGURE 4.4 Theoretical and measured Ra for three cutting tests with different cutting parameters .....	58
FIGURE 4.5 PSD of surface for cutting conditions: $V_c = 3$ m/s, DoC = 25 $\mu\text{m}$ and 40 $\mu\text{m}/$ rev .....	60

FIGURE 4.6 PSD of surface for cutting conditions: $V_c = 3$ m/s, DoC = 25 $\mu\text{m}$ and (a.) 20 $\mu\text{m}/\text{rev}$ (b.) 5 $\mu\text{m}/\text{rev}$ (c.) 1 $\mu\text{m}/\text{rev}$ .....	61
FIGURE 4.7 Profile of Teflon $V_c = 3$ m/s, DoC = 25 $\mu\text{m}$ and 40 $\mu\text{m}/\text{rev}$ .....	63
FIGURE 4.8 20x measurement of the Teflon stamper and average PSD of the profile with $V_c = .03$ m/s DoC=25 $\mu\text{m}$ and $f = 25$ $\mu\text{m}/\text{rev}$ .....	64
FIGURE 4.9 20x measurement of replication with profile and average PSD of the replication .....	66
FIGURE 5.1 Precitech 350 diamond turning machine .....	70
FIGURE 5.2 PMMA ‘top hat’ stamper with 25 $\mu\text{m}$ deep cylindrical recess.....	71
FIGURE 5.3 Profilometer measurement of the 25 $\mu\text{m}$ PMMA ‘top hat’ stamper .....	72
FIGURE 5.4 Comparison of ‘top hat’ stamper (black) and replications (blue and red)...	73
FIGURE 5.5 Profilometry measurements of different ‘top hat’ replications .....	74
FIGURE 5.6 Spherical Teflon Stamper .....	75
FIGURE 5.7 Profile of spherical replication .....	76
FIGURE 5.8 Error between stamper and replica – example case.....	77
FIGURE 5.9 Polynomial error fit 5 mm radial region.....	78
FIGURE 5.10 Shrinkage error from correct M1 prescription over approximately 27 mm .....	79
FIGURE 5.11 Comparison of original error profile (blue) to corrected average (orange)80	

## PREFACE

This was a multi-year project that focuses on a manufacturing technique for the production of freeform optics for imaging systems using UV curable polymers and diamond turned stampers. The work involved numerous diverse research challenges: (1) the choice of a suitable UV curable polymer and stamper combination using adhesion chemistry and empirical testing; (2) alignment of the stamper and the substrate in a UV curing chamber; (3) production and testing of a replication system including a freeform stamper; (4) testing of the replication process and associated metrology; (5) correction for shrinkage of the UV polymer during the curing process. This paper will review the experimental setup and results for the replication systems developed, as well as discuss the evaluation of the replications produced. Chapter 1 will give a brief review of freeform optics and give some background information on processes that are comparable to replication such as precision glass molding and replication of micro lens arrays. Chapter 1 also discusses background on adhesion mechanics and mechanics of diamond turning Teflon. Chapter 2 discusses replication systems that were developed. Chapter 3 outlines the experimental set up and results of the force measurements conducted to better understand the dynamics of the mold release process. Chapter 4 discusses the surface roughness of diamond turned Teflon. Chapter 5 outlines the results of the replication experiments and has an analysis of the shrinkage of the replications and the results of a shrinkage correction. Chapter 6 covers conclusions and future work.

## CHAPTER 1: BACKGROUND AND MOTIVATION

### 1.1 Importance of Freeform Optics

This thesis focuses on a manufacturing technique for the production of freeform optics for imaging systems. To understand the importance of freeform optics in imaging it is important to understand the history of the development of optics and optical imaging systems.

Traditional optics for imaging and other systems have historically been limited by available manufacturing processes and metrology systems. Until the 1980s, optical components including lenses and mirrors primarily had either spherical or conic surfaces [1]. While they are easier to manufacture and measure, optics with spherical surfaces can have inherent spherical aberration and this limits the performance of imaging systems. Combinations of conic sections can have improved performance – for example, the two-mirror Ritchey-Chretien form of telescope developed in the 1920s corrects for both spherical aberration and coma using conic mirrors. Higher order aspheres, introduced by Abbe in 1899 [2], provide more degrees of freedom for the compensation of aberrations. The axial three mirror anastigmat can correct spherical aberration, astigmatism and coma with combinations of three aspheric mirrors. However, aspheric optics add further manufacturing and metrology challenges. Ritchey-Chretien two degree of freedom ultra-precision diamond turning was developed through the 1900s [3] and became a commercially viable and widely available technology in the 1980s. This technology has led to increased use of higher order aspheres in optical systems from the 1980s to the present. Aspheric optics have many advantages but are still axisymmetric. For reflective

systems, this typically requires the system be obstructed: optics in the system will block the light collected by the system. An unobstructed system requires that the optics no longer have a common axis, and this then introduces astigmatism. Compensation of astigmatism and other aberrations in a non-axisymmetric system cannot be done with axisymmetric surfaces alone. Hence the drive for so-called freeform optics.

Freeform surfaces as defined by Fang et al. [4] have no axis of rotational symmetry. Freeform optics are optics using freeform surfaces and have many potential benefits such as: increased optical performance, aberration correction, the ability to increase the field of view, as well as decreasing the volume, mass, and number of optics in a system [4], [5]. However, the manufacturing of freeform optics requires more than two degrees of freedom and so traditional optical manufacturing techniques are limited. In the 1980's non-axisymmetric laser components were polished by hand but were expensive and poor quality. The concept of coordinated axis turning to produce non-axisymmetric components was shown to be mathematically possible by Thompson in 1976 at Lawrence Livermore [6] and this was demonstrated experimentally by Douglass in 1983 [7]. However, at that time the electronics and control systems were not developed enough to accurately drive the slides. Coordinated axis turning reappeared with the development of more powerful machine controllers and linear motor drives and this has renewed the interest in using freeform optics in design

The advances of the freeform design, manufacturing and metrology have been associated with "A Revolution in Imaging" [1]. The optical capabilities of freeform optics go beyond what is possible with traditional optics such as the variable zoom of the Alvarez lens design [8] and now the capabilities to manufacture such systems are

available [9]. The freeform revolution still has one major downside. Manufacturing with multiple degrees of freedom ( $>2$ ) is time consuming and this drives increased cost. It was noted by Thompson [6] that in coordinated axis turning, the spindle speed must be low enough to accommodate the coordinated motion of the linear machine axes which often have very limited bandwidth. Even with advances with higher bandwidth fast tool servo systems, the process of turning freeform optics is slow. Freeform milling using three linear degrees of freedom is an alternative, but this process still requires further research to increase its speed [10]. The implementation of freeform optics could be expanded if a less expensive volume production process with the near the accuracy of ultra-precision machining was developed. There are several technologies that could fill this gap.

## 1.2 Precision Glass Molding

Precision glass molding (PGM) has evolved into a viable path for low-cost volume manufacturing of high-quality glass freeform optics. Because it is a competing process to the one examined in this thesis and certain aspects of PGM such as adhesion, coatings, and error compensation are similar to the issues encountered in this work, we provide an overview of the development of the PGM process here. Karow has an overview of optical glass manufacturing processes of the time and describes molding of aspheric optics [11]. Yi and co-workers [12] developed an apparatus for compression molding of glass, a process that later evolved into precision glass molding (PGM). The work was extended with experimental evaluation of adhesion forces and coatings in PGM by Fishbach et al. [13]. Wachtel et al. [14] evaluate the performance and accuracy of a benchtop PGM machine highlighting thermal effects. Mosaddegh and Zeigert [15] measured friction forces in PGM and the reduction of both adhesion and friction forces in PGM has led to

significant work on mold coatings. Coating technology and coating evaluation methods for PGM was studied and reviewed in detail by Klocke et al. [16]. He et al. [17] studied graphene coated silicon molds for PGM and Berhardt et al. [18] developed diamond like coatings for PGM. Simmons et al. [19] have developed inserted PGM processes where the optics are integrated with alignment and fixturing elements of another material and have also done manufacturability studies on PGM versus other manufacturing methods [20]. Gurganus et al. [21] have demonstrated the first replication of high-aspect ratio freeform optics by PGM. The work on PGM is very relevant to the work presented here as it is: (1) a competing technology for mass production of freeforms; (2) requires coatings to decrease adhesion; and (3) requires freeform metrology and correction that is typically empirical [22].

### 1.3 Replication of Optics and Micro-Optics

Another related technology is the production of micro-optics and diffractive optics either by direct micro- or nano-replication of polymers [23] or the replication or patterning of UV-polymers as a photoresist followed by lithography. O'Shea et al. [24] provide an excellent description of the fabrication methods for diffractive optics. Many of the issues encountered with nanoimprint lithography and micro-molding of a photoresist followed by subsequent etching are similar to those encountered in this research. In particular, the application of a UV-curable polymer to a substrate, the patterning of the polymer with a micro-mold, and the subsequent curing of the polymer followed by the release of the micro-mold is a complex process requiring alignment, curing and release that is similar to the process proposed in this thesis for generating freeform optics. We leverage that work as

much as possible here and extend it to the replication of a freeform corrector in a UV-polymer on a curved glass substrate with a freeform stamper.

Replications of aspheric corrective lenses on glass substrates with the best fit radius have been around since the early 1980's [25] and chromatic aberration corrected replicated aspheres are commercially available. The process of replicating aspheres for mass production is well characterized and well understood [26]. The interaction between the UV-polymer and the glass substrates was tested and understood, and bond promoters were used to ensure that the replicant would adhere well to the substrate and not the stamper. UV-transparent quartz molds were ground, and release agents were applied so that the surface energy would be decreased and the replications would release properly. The shrinkage characteristics of the photopolymer were characterized and the molds were corrected for shrinkage. This process was well developed for aspheric optics and can be applied to freeform optical replication. The molds used for the replication of aspheric optics in this work were quartz. For the work presented here, this was not a viable path. Grinding of brittle materials such as quartz is well understood [27] but three axis sub aperture freeform grinding of quartz is not well understood. While there is also work on the single point diamond turning of quartz [28], the tool wear is prohibitive. In this work, the freeform stamper was machined by coordinated axis diamond turning and the substrates were UV-transparent glass spheres. Freeform surfaces were generated on a near net shape transparent substrate using UV curable polymers.

Because it has been shown that UV-polymers can be used to replicate structured optical surfaces including diffractive optics [24], it is a natural conclusion that UV polymers can also be used to produce a thin freeform optical corrector on a substrate.

However, the fact that high fidelity microscale features can be replicated also means that the surface roughness and mid-spatial frequency errors present in the stampers will be replicated into the optical surface and will effect image quality [29] of the replicated optics. Thus, the surface roughness, mid-spatial frequency errors and the figure of the stamper must be well controlled to produce a high-quality optic. To maintain the quality of the stamper, the goal was to manufacture the stamper with well-controlled coordinated axis diamond turning.

#### 1.4 Conceptual Approach to Freeform Replication on a Near-net-shape Substrate

The process proposed for the mass production of freeform optics in this thesis is a hybrid process related to PGM, injection molding of plastics, and wafer level replication of optics. The proposed process is based both on optical design considerations and on manufacturing. Many freeform optical designs utilize optics with small deviations from a base spherical shape and even smaller deviation from a base toroidal shape. More specifically the motivation for this thesis was the design of a miniature imaging spectrometer by Reimers *et al.* [30]. In this design a classical Offner-Chrisp spectrometer design is miniaturized by a factor of five by converting the primary and tertiary mirrors in the design to freeform optics and combining them with a convex spherical grating. The primary and tertiary mirrors are primarily toroidal with higher order freeform terms to correct aberrations. Inexpensive manufacturing of these optics was the driving application for this work. However, when fully developed, the process would be applicable to other freeform optics as well. While we target reflective freeform optics (freeform mirrors) in this work, it may also be possible to replicate transmissive freeform optics. Because of the ability of the process to replicate micro- as well as macro-features

it may be possible to also replicate spherical gratings such as that in the spectrometer design of Remiers *et al.* [30] or even freeform gratings with a similar process.

The proposed process is shown schematically in Figure 1. The process begins with a glass substrate, either spherical or toroidal, that is near to the shape of the final desired freeform surface (i.e. near-net-shape substrate). Next, a UV-curable polymer is applied to the surface of the substrate. A freeform stamper manufactured with coordinated axis diamond turning is then mated with the substrate maintaining a small gap ( $\sim 100 \mu\text{m}$  or less). The polymer is then exposed to UV light through the UV transparent glass substrate and cured. The stamper is released leaving a freeform corrector on the near-net-shape glass substrate. The surface is then metal coated to produce a reflective freeform mirror.

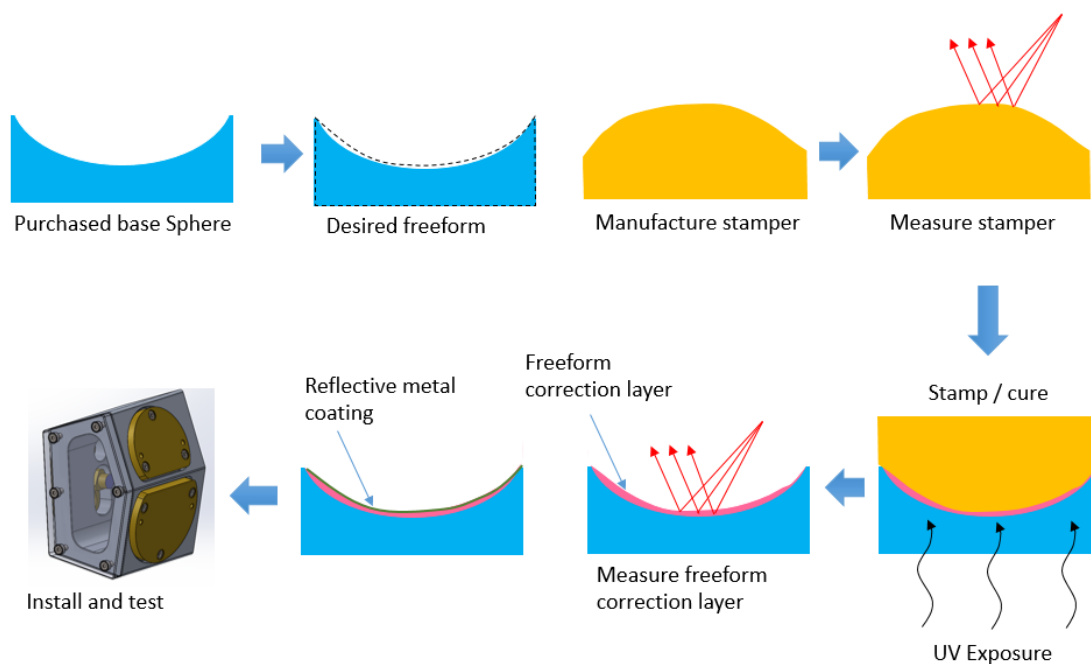


Figure 1.1 Original concept

This work involved numerous diverse research challenges: (1) the choice of a suitable UV curable polymer and stamper combination using adhesion chemistry and empirical testing; (2) alignment of the stamper and the substrate in a UV curing chamber; (3) production and testing of a replication system including a freeform stamper; (4) testing of the replication process and associated metrology; (5) correction for shrinkage of the UV polymer during the curing process.

Before moving on, a practical comment must be made about the near-net-shape substrates used in this research. It was conceptually appealing to use a toroidal substrate so the freeform corrective layer could be made thinner. However, the practical challenges associated with the alignment of a toroidal substrate with a freeform stamper and the increased cost of producing accurate toroidal substrates in glass made it clear that the better approach was to use a spherical substrate with a slightly thicker freeform corrective layer. Accurate spherical substrates are readily available as plano-concave or plano-convex glass lenses. Thus, from here on it is assumed that the glass substrate is spherical and not toroidal.

These research challenges and the results obtained in the development of this replication process are the subject of this thesis.

### 1.5 Adhesion Mechanics

Successful implementation of the replication process conceptually outlined above requires some understanding of adhesion mechanics. For the process to be successful the UV-curable polymer must bond to the substrate and not remain adhered to the stamper, as is well known in the nano-imprint lithography and micro-optic lithography literature, this

is not a trivial problem. Unlike most other research, this process utilizes a curved substrate and stamper further complicating the adhesion problem.

Adhesion is defined as the propensity of two dissimilar materials to cling or stick to one another. The various theories of adhesion are complex, but it is generally accepted that there are five main mechanisms for adhesion which are more or less active depending upon the situation. The five mechanisms are: (1) chemical; (2) mechanical; (3) dispersive adhesion; (4) electrostatic; and (5) diffusive.

Chemical adhesion occurs when two materials form a new chemical compound at the interface. Mechanical adhesion occurs when two adjoining materials form a mechanical interlock on a small scale. Velcro bonds mechanically and the sewing of two materials together can be viewed as mechanical adhesion. Mechanical adhesion can also be used to bond chemically inert materials such as polytetrafluoroethylene (PTFE) or Teflon to other materials; such mechanical interlocking at the surface level is exploited in the manufacturing of non-stick pans. Dispersive adhesion occurs due to van der Waals forces, attractive forces between two materials that originate at the molecular level. This is a complex process with many potential physical mechanisms and its relative strength is affected by many factors including chemical composition, wetting, surface roughness and macroscopic shape. The adherence of a gecko lizard to surfaces is largely attributed to van der Waals forces enhanced by microscopic hairs on their toes. Electrostatic adhesion occurs when two materials build up positive and negative charge that is not dissipated and causes them to attract. A balloon given a charge by rubbing it on hair adheres to a wall or ceiling due to electrostatic adhesion. Diffusive adhesion occurs when two materials have molecules that are mobile and mutually soluble in one another. This

occurs in sintering processes where, for example, metal and ceramic particles are brought into contact under high pressure and temperature, causing atoms from one particle to diffuse into neighboring particles. The work of Awaja *et al.* [31] has a comprehensive review of the mechanics of adhesion due to these various mechanisms.

Adhesion mechanics and factors that lead to the forces between materials is a very complex issue and the examination of these factors extends beyond the scope of this work. However, for the purposes of this work, surface energy provides a useful quantification of the adherence of materials by multiple effects. Thus, in this thesis empirical approaches guided by the concept of surface energy are used to quantify adherence and, in the end, choose suitable materials for the freeform replication process. The experimental results from later chapters will discuss the effects of surface roughness as well as surface energy as they pertain to the desired results.

### 1.6 Teflon Turning Mechanics

PTFE is a material of interest for molding due to its high lubricity, inertness and low surface energy which promotes mold release. Thus, it is examined as a material that can be directly diamond turned to produce a freeform mold. However, the generation of a surface in polymers can be complex due to material behavior and is thus investigated in this thesis.

Diamond turning has been used to produce optical surfaces for decades and for so-called diamond turnable materials [32] the generation of the surface is primarily a geometric process. A periodic cusp structure is generated on the surface by a round-nosed diamond tool feeding over the surface. The surface structure scatters light at predictable angles and this scattering can be modeled [33]. The surface roughness produced by

diamond tools with circular radii have been modeled analytically, and the closed-form solutions for roughness parameters of theoretical profiles that represent the periodic structure of diamond turned surfaces have been developed [34]. With an understanding of the theoretical roughness of diamond turned surfaces, the necessary cutting parameters can be determined from the desired surface roughness for typical materials. Carr *et al.* [35] observed that for typical materials, environmental and process parameters have the most influential effect on the surface roughness. But, for polymers, the physical and chemical properties are the limiting factors in the surface finish [35]. It is important to understand the viscoelastic property of polymers during cutting operations as they determine whether the polymer will deform plastically or elastically when being cut. The time-temperature superposition principle describes that, for a polymer at a constant temperature, the response to a given disturbance depends on the relaxation time of the polymer. For a disturbance applied at a certain rate, the relaxation time decreases with increasing temperature. In diamond turning situations, it is generally accepted that temperatures are low due to the high conductivity of the diamond. However, polymer materials have low conductivity and are affected by lower temperatures so both thermal and mechanical effects may be active in polymer turning. Cutting speed will affect both temperature and strain rate. The strain rate must be compared to the relaxation time of the polymer at a given temperature to determine its response. If the strain rate is high compared to the relaxation time, the polymer will behave elastically. If the strain rate is low compared to the relaxation time, the polymer will behave plastically. The response will determine the character of the surface produced [35]. In this thesis we examine diamond turned Teflon/PTFE by varying process parameters and examining the surface

roughness. If adequate surface finish can be achieved on a PTFE substrate, it could be a suitable material for replicating complex optical components due to its beneficial material properties.

Electroless nickel phosphorus (Ni-P) has been used as tooling to replicate optics because it is easily diamond turnable and produces excellent surface finish, but it does not have longevity due to the adhesion forces during the molding process [36]. It has also been seen that PTFE can be suspended in Ni-P resulting in an evenly distributed matrix. It was shown that the Ni-P-PTFE sample was more hydrophobic than the Ni-P sample, but it is unclear whether the same surface finish could be achieved with Ni-P-PTFE. It was also unclear whether this helped the longevity of the mold.

## CHAPTER 2: KINEMATICS OF REPLICATION

### 2.1 Introduction

This section will discuss the different alignment configurations that were used to align the stamper and the substrate for replication. The results of the replications will be discussed in a later section.

### 2.2 Experimental Setup

The replication process was refined over the course of the project and the major subsystems developed will be discussed.

#### 2.2.1 Background

As was previously stated in Chapter 1, the work of Sohn and Dow [37] provided an important starting point for the work developed in this thesis. Sohn and Dow proposed, we believe for the first time, the idea of using a thin film of UV curable epoxy that was cast on an optical surface with a large form error using a diamond-turned mold. Similar to the process developed here, Sohn and Dow [37] describe a substrate consisting of a glass or plastic optic having large form error on the order of 50  $\mu\text{m}$  to 100  $\mu\text{m}$  over a clear aperture on the order of 100 mm diameter. Planar diamond turned nickel and aluminum masters were then used to mold a UV curable epoxy, Summer Laboratories J-91, to a flat glass substrate with thicknesses ranging from 50  $\mu\text{m}$  to 100  $\mu\text{m}$ . The epoxy is cured by UV exposure through the glass substrate. The researchers also model and measure form errors in the flat molded surface. They assume these errors are due to tensile stresses in the thin film of the molded and cured epoxy that cause a bending of the substrate and produce a form error dominated by power. The form errors in the optical

substrate with the molded thin film produce a convex shape that is thicker in the middle and thinner toward the outside edges, with a total PV of 20  $\mu\text{m}$  over a 100 mm circular flat. These form errors are corrected to approximately 1.5  $\mu\text{m}$  using a corrected convex spherical mold with a 250 m radius of curvature. Because the authors assume the errors are due to stress induced part distortion, they are surprised by the convex form errors which they conclude must be due to an 0.3% expansion of the epoxy on curing. In our work with thicker substrates, we have shown that this form error is due to volumetric shrinking of the epoxy on curing by approximately 2%. This work provided a starting point for our work: use of metal stampers with Summers Optical J-91 polymer.

### 2.2.2 Preliminary Identification of Stamper Material

Based on the work of Sohn and Dow, our initial experiments tested stampers made of three different materials used to mold the epoxy onto a flat flint glass microscope slide. The initial tests were conducted to select a material that could be diamond turned for use as the stamper in the replication system and would not adhere to the epoxy on release.

The materials tested were aluminum, brass, and copper. The first stamper geometry was a diamond turned flat. The initial tests were conducted by applying the UV-polymer directly to the stamper and then positioning the glass substrate on to the stamper by hand. The gap between the stamper and the substrate was not constrained and the thickness of the cured polymer layer was approximately 150  $\mu\text{m}$ . This could be changed by manually increasing or decreasing the amount of UV-polymer applied to the stamper. The amount of polymer was not measured in the initial tests. These initial replications released well with the aluminum stampers.

To test release for more complex, and nominally freeform geometries, the next set of stampers had a low amplitude sine wave turned on the surface. Figure 2.1 shows stampers diamond turned in copper, brass, and aluminum. The replications released easily from the aluminum stamper but broke the glass substrate during release on the copper and the brass stampers. From this preliminary result, aluminum was initially chosen for the stamper material.



Figure 2.1 Copper, brass, and aluminum stampers with sinewave

### 2.2.3 Initial Evaluation of Controlled Replication and Shrinkage

Based on the previous initial results, another exploratory experiment was completed with two main goals: (1) to evaluate the ability of the process to replicate a complex pattern under controlled gap conditions; (2) to evaluate the possibility of generating voids due to non-uniform epoxy flow between the stamper and the substrate; and (3) to estimate the shrinkage in the polymer on curing. To meet the goals of the experiment, a stamper was diamond turned in Aluminum 6061. An axially symmetric sinusoidal feature with a programmed peak-to-valley amplitude of  $\pm 5 \mu\text{m}$  was diamond turned into the surface. To control the overall thickness of the replicated feature, a raised

annular rim was turned on the outer diameter of the stamper with a height of 100  $\mu\text{m}$  relative to the mean height of the sinusoid.

The experimental sequence is shown in Figure 2.2. The polymer was applied to the stamper with the volume only roughly controlled manually. A glass slide was then placed on top of the stamper and polymer material and allowed to rest on the rim of the stamper. The polymer completely filled the gap with no visible voids except at the one edge (see Figure 2.2 (c)). The stamper and slide were then placed in an ELC-500 UV Cure Chamber available from Fusionnet LLC and exposed to UV radiation at a wavelength of 365 nm for 10 minutes until fully cured (for full specifications see: <http://fusionnet.com/Item/ELC-500-UV-Cure-Chamber>).

Comparative measurements were made on the stamper and two replicas on the Zygo NexView scanning white light interferometer with the 2.75x objective with half zoom lens (approximately 6 mm square field of view). Piston and tilt were removed from the measurements, but no filtering was done as this might affect the amplitude estimates.

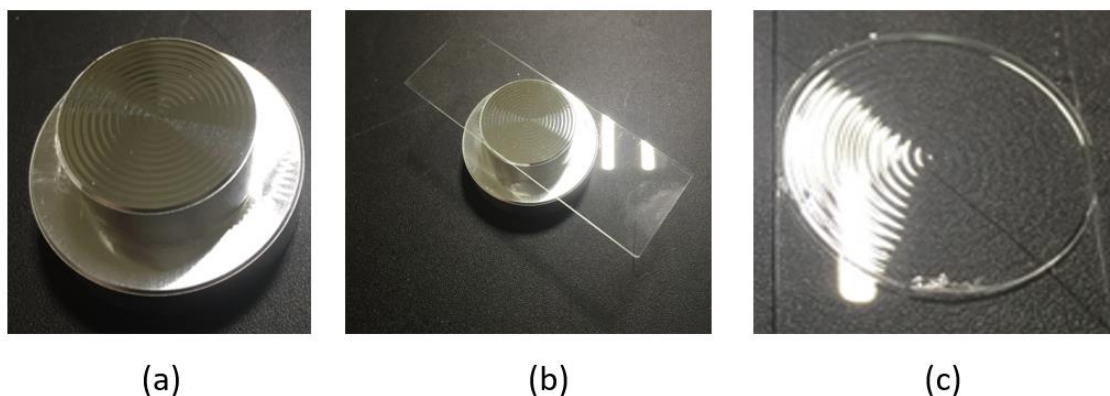


Figure 2.2 Replication process showing (a) aluminum stamper with a controlled sinusoidal feature; (b) glass slide on rim of stamper with polymer fill prior to curing; and (c) fully cured polymer on glass slide with some visible edge defects.

The sine wave amplitude was estimated from measurements made at five locations on the stamper and each replica were measured to estimate the shrinkage. Example measurements of the stamper and one replica are shown in Figure 2.3 (a) and Figure 2.3 (b). The images show that the replica is the inverse of the stamper. Figure 2.3 (c) shows estimates of the amplitude of the sine wave on the stamper versus the two replicas. There appears to be a systematic difference between the measurements. The amplitude of the sinusoid on the stamper is estimated at  $9.878 \pm 0.048 \mu\text{m}$ . The amplitude of the sinusoids on replicas 1 and 2 are  $9.740 \pm 0.050 \mu\text{m}$  and  $9.781 \pm 0.041 \mu\text{m}$  based on 15 samples. The difference is assumed to be caused by shrinkage ( $\varepsilon$ ) in the polymer during curing. It is estimated by taking the difference between the amplitude measurement on the stamper ( $A_s$ ) and the mean amplitude measurement on the replicas ( $A_r$ ) and dividing by the mean amplitude on the stamper as given in Equation 2.1.

$$\varepsilon = \frac{A_s - A_r}{A_s} \quad \text{Equation 2.1}$$

The mean shrinkage for replicas 1 and 2 are 1.4% and 1.0% respectively. By taking the maximum and minimum amplitude values based on the measurements and uncertainties we can estimate the maximum and minimum shrinkage values respectively.

$$\varepsilon_{max} = ((9.878 + 0.048) - (9.740 - 0.050)) / (9.878 - 0.048) = 0.024$$

$$\varepsilon_{min} = ((9.878 - 0.048) - (9.781 + 0.041)) / (9.878 + 0.048) = 0.0008$$

The shrinkage reported by the manufacturer is less than 2%, our estimates appear reasonable, but the uncertainty is high. If we were to take a predictive approach to mold

correction for shrinkage, we would require further controlled experiments to identify it with less uncertainty. Also, the shrinkage evaluation here is along one linear dimension while true shrinkage will be volumetric. However, as will be demonstrated later, our approach to correcting the mold to control optical form will be empirical and not predictive. Thus, the estimate is sufficient for our purposes here.

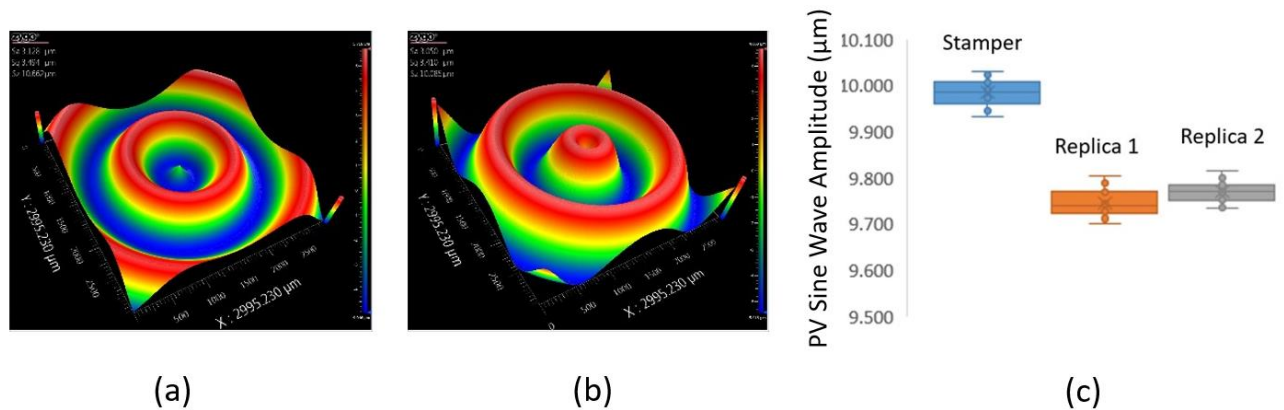


Figure 2.3 (a) Sample scanning white light interferometer measurement of the stamper; (b) Sample scanning white light interferometer measurement of replica; and (c) mean and standard deviation of 15 sample PV amplitude measurements of sine wave on stamper and two replicas.

## 2.2.2 Automated Replication System

Once aluminum was chosen as the stamper material, a system was developed as a senior design project to automate the replication process. The automated design and material testing were done by Zachary Geiser and Zachary Muller.

The system utilized ball and groove kinematic mounts on platens to position the stamper with respect to the glass substrate and to constrain the gap between the stamper and the glass substrate. The stamper was mounted on one platen and the glass substrate was mounted on the other. The substrate platen had an aperture to facilitate UV exposure. The replication system utilized a stepper motor on a screw drive to actuate the stamping

motion. The target of the kinematic mounts was to constrain the gap at  $50\ \mu\text{m}$ . The automated replication system with kinematic mounts can be seen in Figure 2.4.

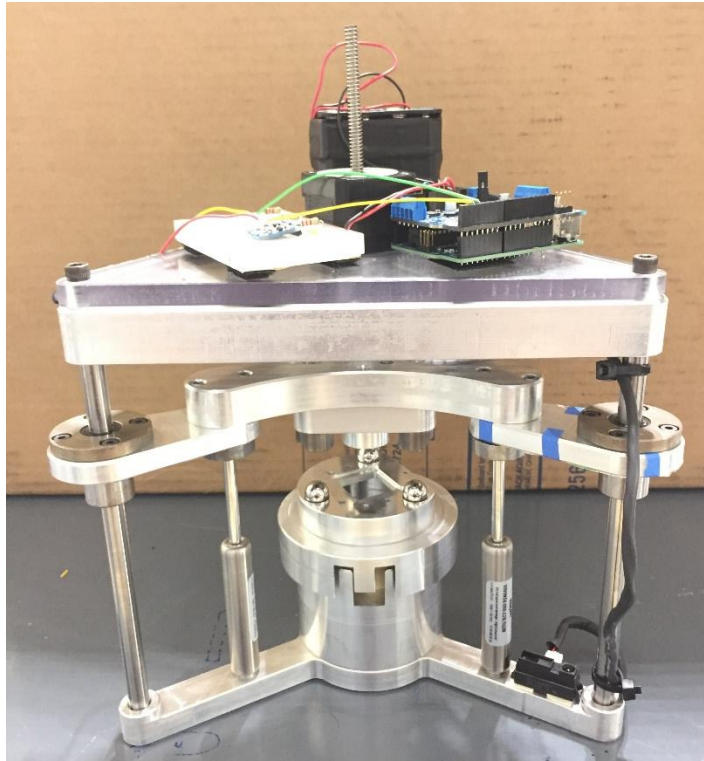


Figure 2.4 Replication system using kinematics alignment and stepper motor drives

The initial objective was to use thin polymer layers on substrates that were the base radius or base toroid of the prescription. The initial freeform selected had deviation from base toroid of  $30\ \mu\text{m}$ . The initial tests with the kinematics were intended to replicate layer thicknesses of  $50\ \mu\text{m}$  to work towards layer thickness of  $30\ \mu\text{m}$ . The initial tests with an aluminum flat of  $150\ \mu\text{m}$  with no kinematics released well, but as the layer thickness decreased, the replicated material started to tear and release forces increased. The replication process was then re-evaluated with manual actuation to help better understand the release process.

### 2.2.3 Triangular Kinematic Replication System

This revised kinematic replication system was designed with the help of Dustin Gurganus and machined by Nick Horvath. The replications were done using platens with kinematics shown in Figure 2.5.

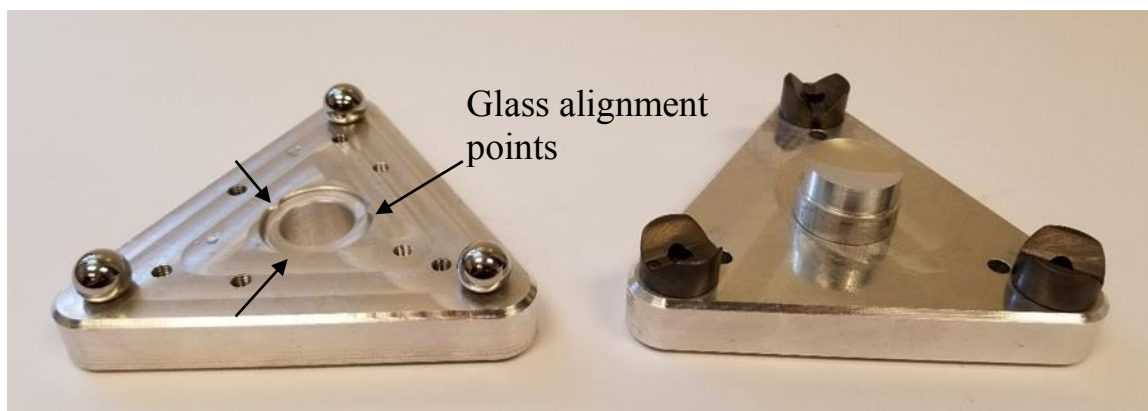


Figure 2.5 Kinematic replication system with spherical aluminum stamper (right) and glass substrate (left).

The configuration shown in Figure 2.5 allows for multiple stamper and substrate combinations to be tested at different layer thicknesses. The left platen would hold the glass or UV-transparent substrate via Crystalbond 555 mounting adhesive, a wax that melts at 50 degree Celsius, so that the glass could be mounted and removed by heating. There are three alignment points in the circular relieved area in the substrate holder, designed to center the circular glass substrate during wax mounting. An aperture through the back of the platen allows the substrate and replicant to be illuminated with UV light for curing. For transportation to and from the curing chamber without unseating the kinematic mounts, three bolts were used to preload the mounts.

The stampers were mounted into the other platen using M3 hardware and alignment pins for stampers that are non-axisymmetric. In a production setting, the gap

between the stamper and the substrate would be changed by cutting a stamper to the correct thickness. In testing, the gap thickness was varied by shimming the stamper in three places between its base and the platen.

The gap thickness was first qualitatively verified by a “paper test”. A thin piece of paper (kim-wipe) was placed in between the stamper and the substrate and the gap was adjusted until the paper was pinched and no longer moved. The gap was then verified by measuring replicas. The substrate thickness was measured with a micrometer and the replicated optic was measured. The difference in these two measurements yielded an estimate of the thickness.

This triangular kinematic system was used to test replication of a convex spherical stamper on a concave substrate with a larger radius. The convex stamper radius was 61.69 mm to match the base radius of the target freeform for mirror 1 on the spectrometer design highlighted in Chapter 1. The substrates were inexpensive, plano-concave lenses, with radii of 83.29 mm purchased from Edmunds Optics. The radius of the substrates was chosen to be greater than the radius of the convex stamper in these first sphere-on-sphere replication experiments so that the thickness of the replicant layer was smallest in the center and increased toward the outside edges as shown in Figure 2.6. Figure 2.6 (a) shows a comparison of the stamper and substrate surfaces with a minimum gap set by the kinematic mounts of 150  $\mu\text{m}$ . Figure 2.6 (b) shows the gap as a function of radial position and this increases from the minimum value of 150  $\mu\text{m}$  to a maximum of 350  $\mu\text{m}$  at the outside edges. This configuration was chosen to reduce the chances of trapping air in the gap between the stamper and the substrate.

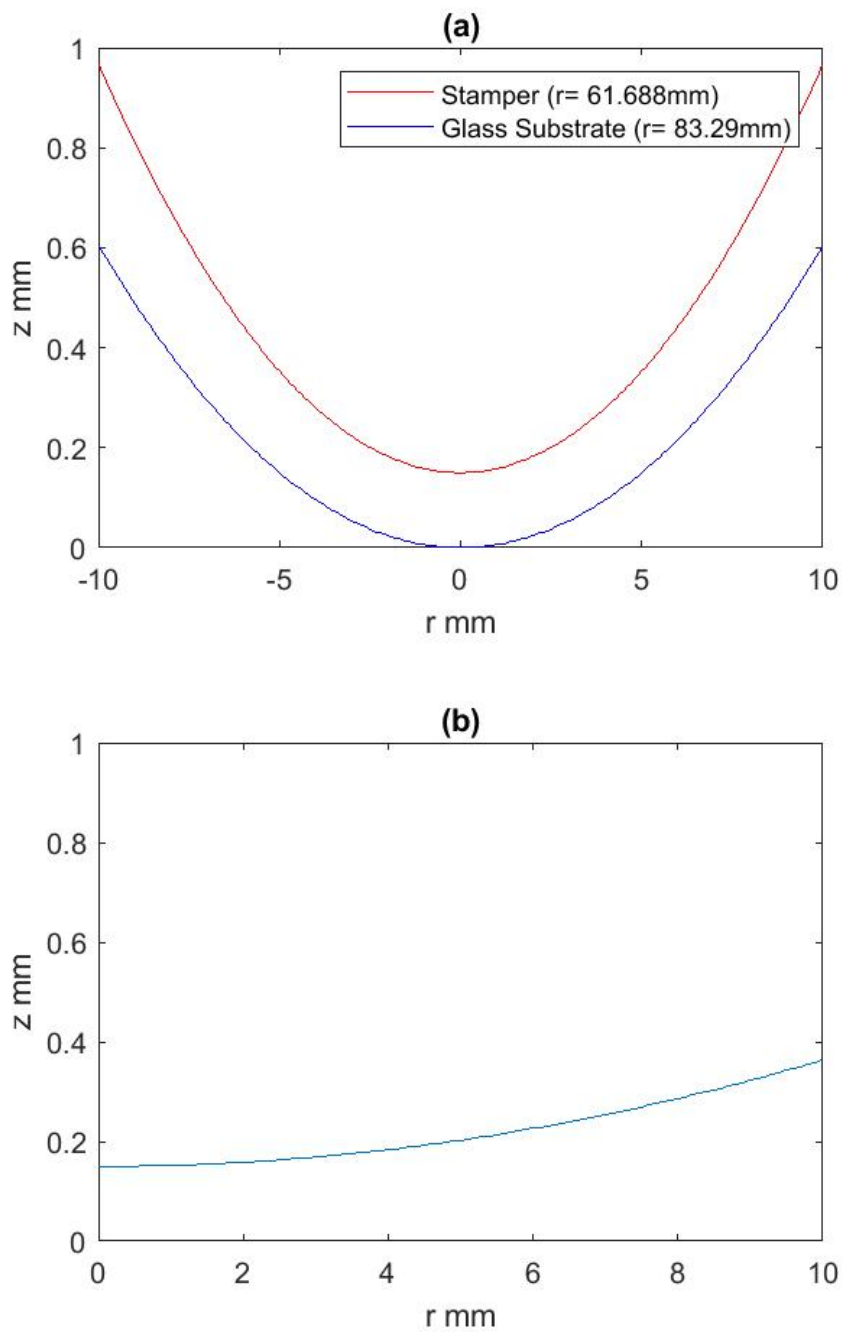


Figure 2.6 (a) Plot of stamper and substrate base radius (b) shows the gap as a function of radial position  $r$  (mm).

The triangular replication system geometry was beneficial during the release process as it could act as a hinge, pivoting on two of the ball and groove connections. This hinge motion allowed for the system to be “peeled” apart with a wedge motion. This motion can be more easily visualized using the Kelvin Clamp model as seen in Figure 2.7.

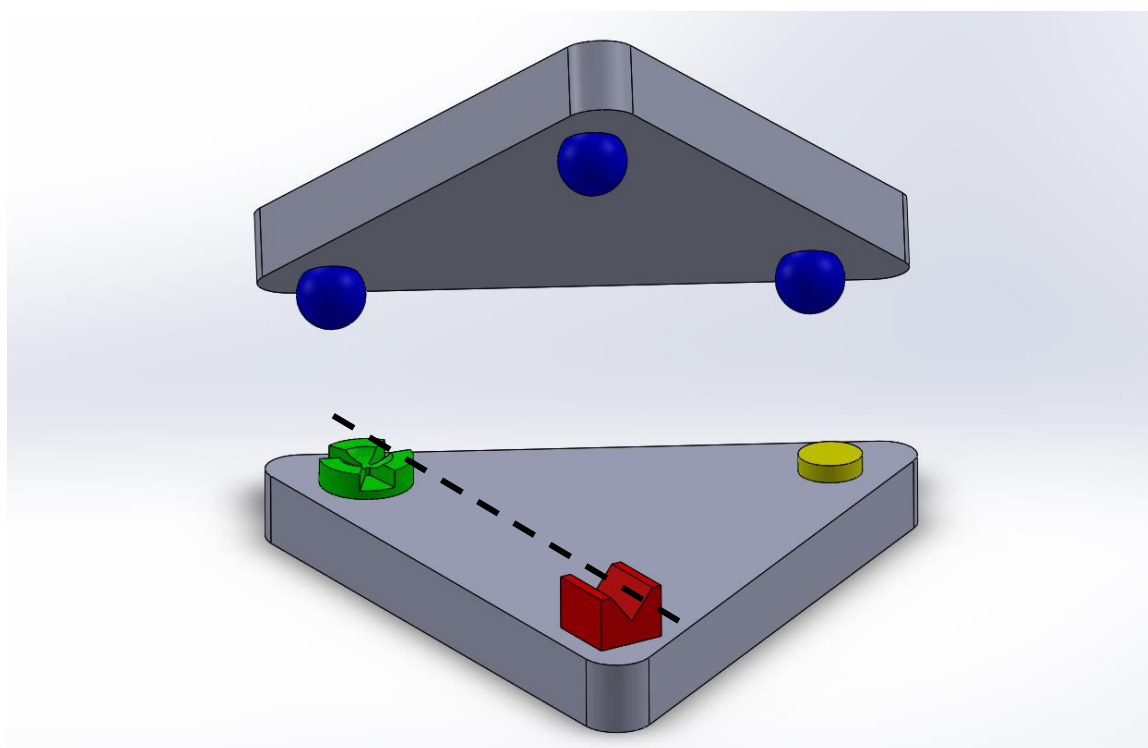


Figure 2.7 Kelvin Clamp model

The concave tetrahedron in green constrains the translation between the plate with the spheres, the V groove in red constrains the rotation about the tetrahedron, and the flat in yellow constrains the tilt between the plates. It can be seen from this model that the top plate can rotate on the spheres about the axis between the V groove and tetrahedron. This

peeling motion produced a high moment on the interface was allowing more efficient release of the mold from the replica.

#### 2.2.3.1 Scope of Work Expanded to Transmissive Optics

As suggested by Sohn and Dow [37], the replication process can also be used to correct transmissive optics because the index of the cured polymer (1.55) is close to that of glass. The losses due to Fresnel reflection at the interface are low – approximately 0.04% at normal incidence for an epoxy glass slide (index of 1.49) interface. To test this hypothesis, experiments to change the focal length of plano-concave lenses were conducted by increasing and decreasing the radius of curvature of the lens. The effect is qualitatively demonstrated in Figure 2.8. The middle optic is left unchanged. The curvature of the concave side of the optic on the right is decreased (greater radius), increasing the focal length. The curvature of the concave side of the optic on the left is increased (lesser radius), decreasing the focal length.

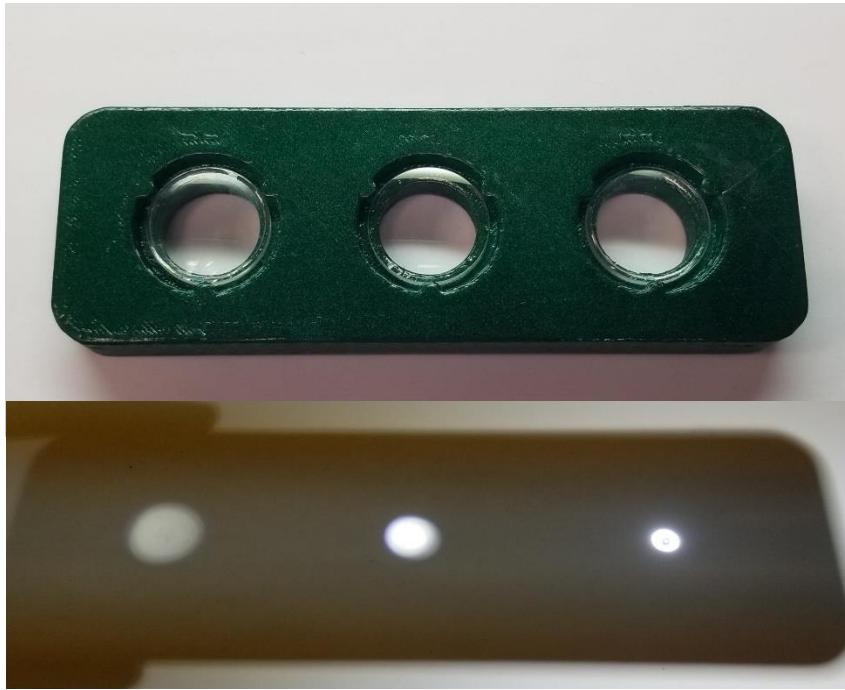


Figure 2.8 Three optic demonstrator with increased focal length/decreased power (left) original lens substrate (center) and decreased focal length/increased power (right)

The triangular kinematic system was difficult to operate due to its shape and was easily decoupled reducing the repeatability. This decoupling could damage the diamond turned stamper or break the glass substrate. This decoupling issue and the stack up uncertainty of the interchangeable stamper lead to a design revision of the replication system.

#### 2.2.4 Replication System with Spacer Ring

The next iteration of the system, shown in Figure 2.9. The outer diameter of the stamper and substrate are 63.5 mm. The system utilized a 12.7 mm thick spacer ring to define the gap between the stamper and the glass substrate. This spacer was incorporated as a separate component so the replicated layer thickness could be decreased or increased by either turning the faces of the spacer ring or by changing to a thicker or thinner spacer

ring. The system can be simplified to two components by incorporating the spacer into either the stamper or substrate holder, depending on the application.

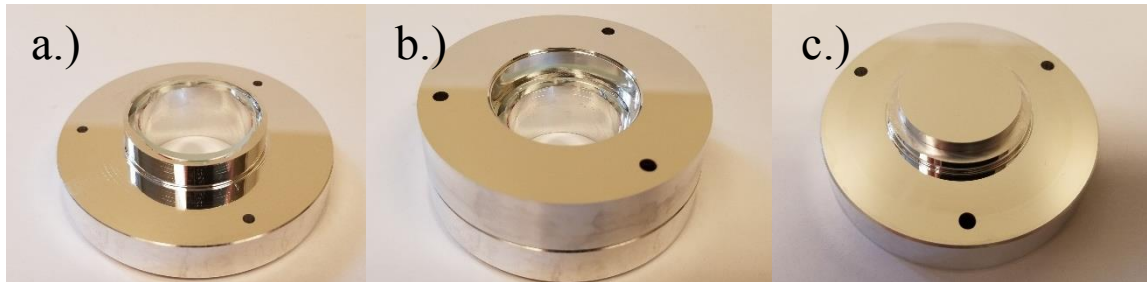


Figure 2.9 New replication system using spacer ring comprising substrate holder a.) spacer ring b.) and stamper c.)

The replication system using a spacer ring simplified the system and was designed to increase the repeatability of the replication process. The system was first machined on a HASS CNC milling machine. Then the mating surfaces and the spacer ring were diamond turned on a Moore Nanotechnology 350-FG. The critical dimensions that defined the gap between the stamper and substrate, and thus the replicant thickness, were the thickness of the spacer ring, the distance from the surface of the glass substrate to the mating flange, and the distance from the stamper face to the stamper mating flange. Another critical factor is centration of the stamper and the substrate holder. This was controlled by diamond turned bore in the stamper, which mated with the diamond turned outer diameter of the raised substrate platform on the substrate holder and the raised section of the stamper. The system could be further constrained with a pin to control clocking for freeform optics. A cross section of the design and the various features controlling the assembly tolerances can be seen in Figure 2.10. It is estimated that with this procedure, the gap and in-plane centration of the stamper and the substrate holder can

be controlled to  $\pm 1 \mu\text{m}$  in a temperature-controlled environment,  $\pm 0.1 \text{ }^\circ\text{C}$  in the diamond machining laboratory.

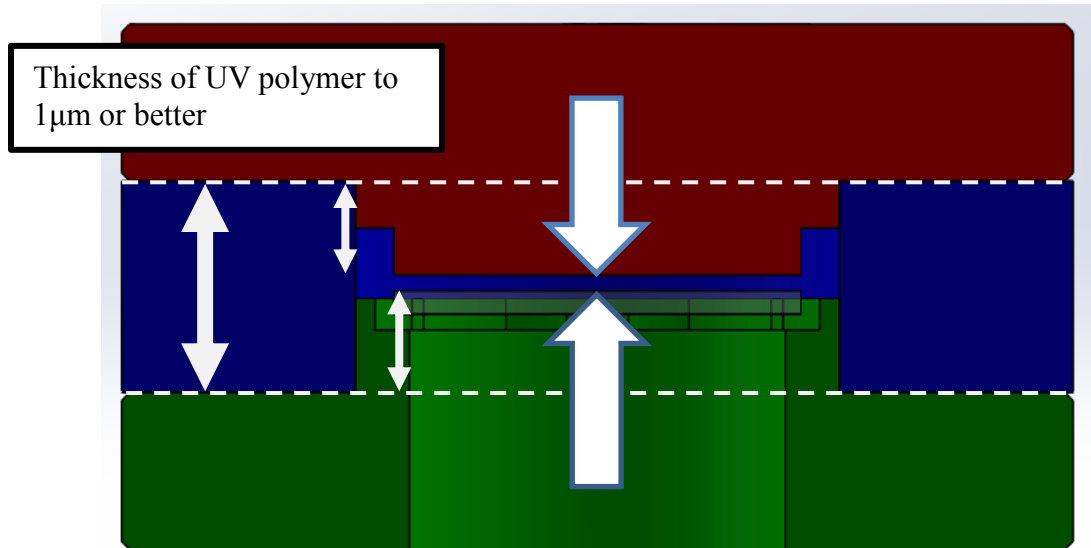


Figure 2.10 Cross-sectional view of the replications system showing stamper (red), spacer (blue), and substrate holder (green)

The cross section shows the gap between the glass substrate and the stamper face which defines the layer thickness of the UV polymer layer. The glass substrate was held into the substrate holder using high temperature wax to ensure that the glass was seated properly in the housing. The housing was designed with three positioning nodes to center the glass and had three pads for the glass to sit on for exact constraint. The pads were diamond turned to ensure they were at the same height and square with the axis of the bore of the substrate holder. The substrate holder can be seen in Figure 2.11.

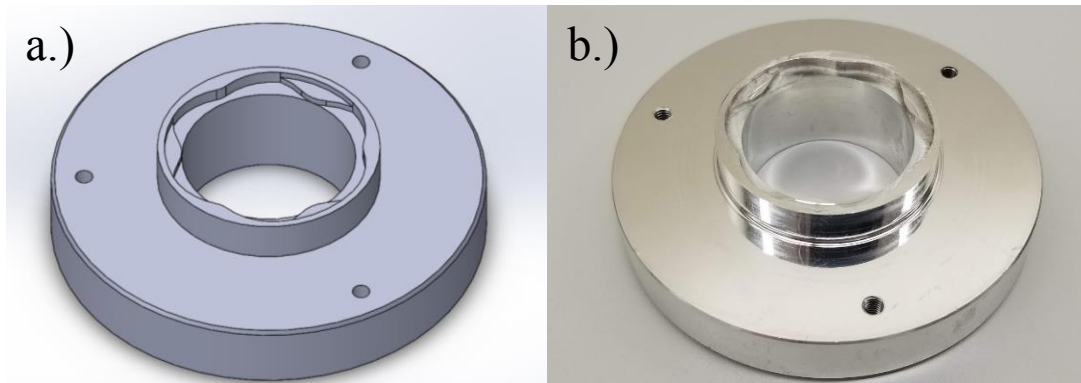


Figure 2.11 Substrate holder CAD a.) model and finished part b.)

The outer diameter of the substrate holder was diamond turned to interface with the diamond turned bore of the spacer ring and the diamond turned outer diameter of the stamper. The new system constrained the motion linearly along the optical axis due to the precision bores.

The advantages of this new system are simplicity and the control of critical dimensions with the manufacturing process. Also, if needed, the position of the glass substrate can be measured in the diamond turning machine and the faces can be turned again to account for error in the glass substrate thickness. The disadvantages of the new system are that it is over-constrained (not a kinematic alignment system) and it does not have a lever arm to place large moments on the stamper to facilitate release.

Thus, the new replication system was more effective in quickly aligning the substrate and stamper, however due to the over-constraint it often could not be separated easily after curing. Further, since the spacer ring was turned to the same diameter as the stamper, it made the system difficult to grip during the release process. This was an unexpected issue as in prior tests, release forces were not a problem. Further design revisions were required for testing.

In a relatively simple design revision, the spacer ring was re-machined into three pieces to ensure that it could be removed after the curing process producing a gap where a moment could be applied between the stamper and substrate to facilitate release.

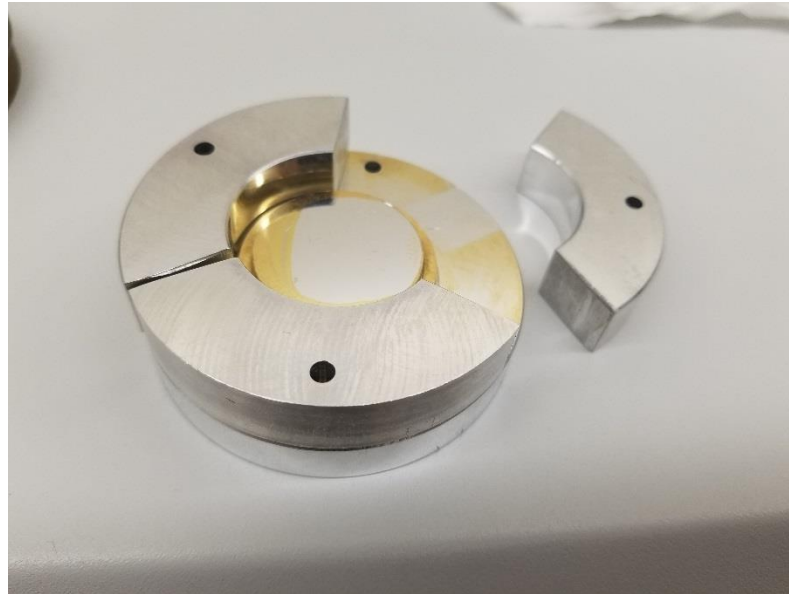


Figure 2.12 Three-piece spacer and gold coated Aluminum stamper

The three-piece spacer shown in

Figure 2.12 allowed the spacer to be removed and the replication to be released using the same peeling motion as before. The replications using the three-piece stamper were moderately successful but raised the issue of release forces and adherence issues. Release force analysis will be discussed in Chapter 3.

### 2.2.5 Replication System with Split Spacer

The replication system with the split spacer was designed after material testing and release force testing were conducted. The stamper material was changed to polytetrafluoroethylene (PTFE) which reduced release forces significantly and nearly eliminated one failure mode in which the replicant remained adhered to the stamper and

not the substrate. The mechanical design for the stamper included a thicker backing so that the part would not distort during fixturing and machining. The final design is shown in Figure 2.13.

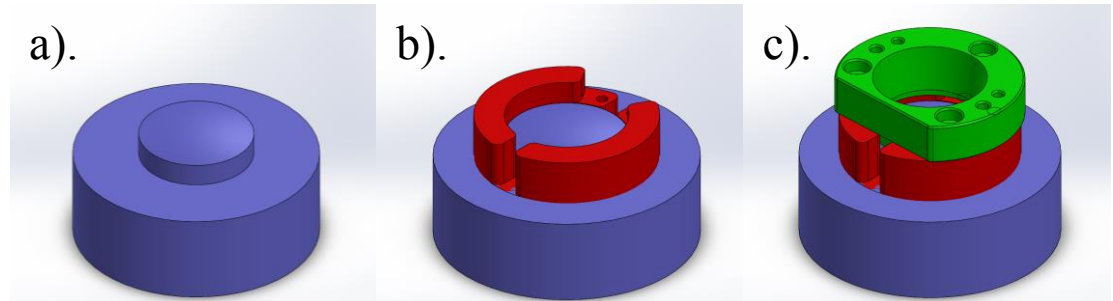


Figure 2.13 Split ring replication system assembly showing a.) Teflon stamper b.) spacer ring c.) substrate holder

A spherical stamper was rough cut on the HAAS TM-1. The stamper was then diamond turned on the Nanotech 350-FG. Traditionally, the ratio of diameter to thickness for parts being held using a vacuum chuck needs to be at least 7 to 1. Due to the low modulus of elasticity of PTFE (approximately 2 GPa), the thickness of the stamper was increased to 34 mm, and with a diameter of 66 mm, this yields a diameter to thickness ratio of 2 to 1. The spacer ring thickness is 13.5 mm and the diameter is 46 mm. The substrate holder is 48 mm in diameter and has the mounting features for the spectrometer from CeFO-1.

The spacer ring was redesigned to ensure that it could be removed after the replicant had cured. The spacer ring can be seen in Figure 2.14 below. The spacer ring was made of aluminum and was rough cut on the HAAS TM-1 as a single component. Holes were then drilled and threaded to accept M2 hardware. The spacer was then mounted on the Nanotech 350-FG using wax and the critical surfaces were turned. The

critical surfaces are the flat and the inner diameter. The flats are the mating surfaces with the stamper and substrate holders. The inner diameter was also diamond turned to ensure that the spacer ring mates the outer diameter of the stamper and substrate holder for centration alignment. Once the flat on one side and the inner diameter was diamond turned, the spacer ring was removed, and the thickness was measured. The part was then flipped over and turned down to the final dimension, separating the two halves. This ensured that the bore was concentric and the parts were the same thickness.

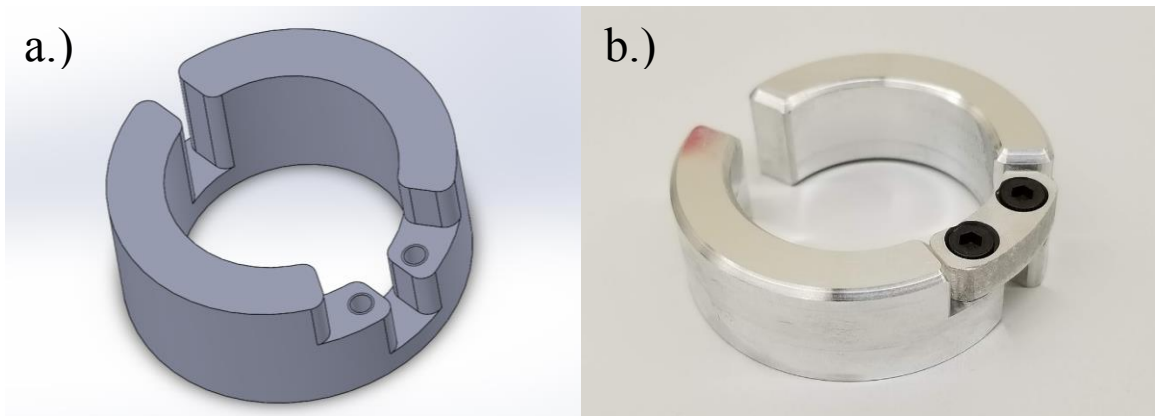


Figure 2.14 Split spacer ring CAD a.) and finished part b.)

The two halves were then held together with a hinge designed to allow each side to make complete contact with the outer diameter and pivot away while the other side maintains contact. This was to ensure that the spacer could be partially or fully removed during the release process.

The substrate holder was designed with features that mate with the housing of the imaging spectrometer in the position of M1 as described in Chapter 1. There are three counter sunk through-holes for M3 hardware for mounting, and two pins to constrain rotation. The substrate holder model and final part before it was diamond turned can be seen in Figure 2.15 below. The substrate holder has a large aperture to allow exposure to

UV light. The substrate mounting features were simplified in this design to reduce manufacturing time. The three pads on the previous design were eliminated to reduce the complexity.

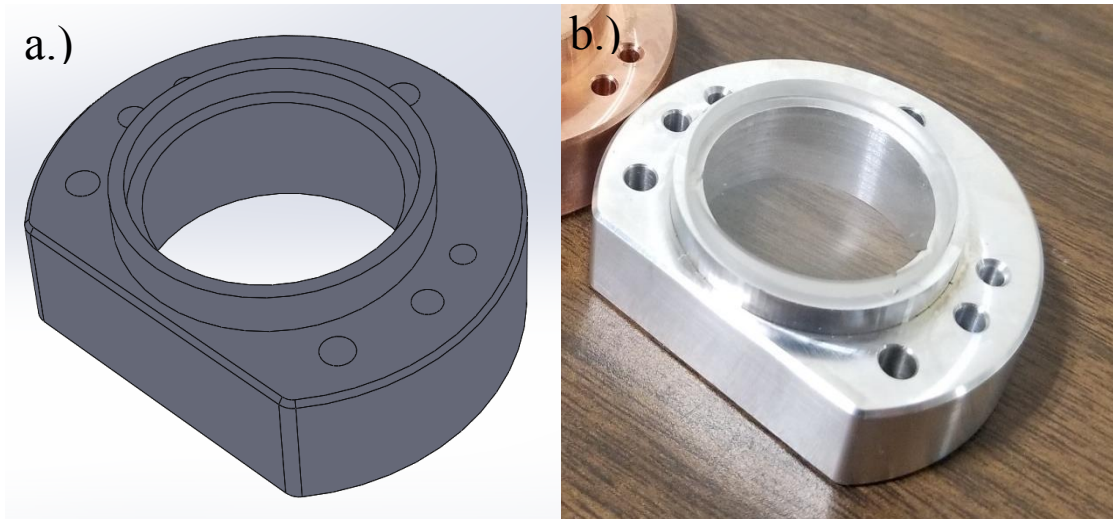


Figure 2.15 Substrate holder with mounting features CAD a.) and finished part b.)

The incorporation of the PTFE stamper greatly increased the repeatability of the replication system and reduced failures. PTFE was selected based on force measurement experiments. The force measurement experiments and replications will be analyzed in the following chapters.

## CHAPTER 3: DYNAMICS OF REPLICATION

### 3.1 Introduction

The process of replication is different from other molding processes, as the UV-polymer does not provide appreciable resistance to deformation until it is cured. However, the polymer is an optical epoxy, and is meant to bond to surfaces once cured. Thus, significant forces are generated when separating the stamper from the polymer and substrate after curing is complete. As previously mentioned, a significant part of the research work was devoted to find stamper and substrate combinations that accomplish two main goals: (1) provide the figure and finish on the replicated optical surface after curing; and (2) promote strong bonding to the substrate and relatively easy release from the stamper. Adhesion is not a simple problem; the complexities of the adhesion process were outlined in Chapter 1.

As described by Ochoa-Putman [38], for strong adhesion, the adhesive must thoroughly wet the surface and, in general, a liquid will more thoroughly wet a solid surface if the surface energy of the adhesive is as low as or lower than the solid surface being wet. Since the polymer has a fixed surface energy in liquid form, the goal of having the polymer adhere well to the glass substrate versus the stamper is more readily accomplished if the stamper material has a significantly lower surface energy than glass ( $\sim 80 \text{ mJ/m}^2$ ). However, the problem is complex as the polymer transforms from a liquid to a solid during the UV curing process and this changes its surface energy. Thus, while we were guided by adhesion physics, and in particular free surface energies of the

materials used for the stamper and the substrate, practicality dictated that we also take an empirical approach to the problem.

To this end, an experiment was developed to measure the forces during release of various candidate stamper materials from the cured polymer. This data was collected to determine suitable material combinations for the replication process. The data collected can also help to optimize the release process and to increase the mold tool life and replication repeatability. Higher release forces increase the potential for damage to the optical surface, and because of uncontrollable factors, this also reduced the repeatability and the success rates obtained in the molding process. When the release force is greater than the adhesion force between the glass substrate and the polymer, separation issues occur.

Lack of repeatability of the replication system when using metal stampers, particularly aluminum as suggested by Sohn and Dow [37], prompted an investigation into release coatings for the replication process and alternative stamper materials.

Coatings and release agents can change the interface mechanics, making the materials more likely to release from the mold rather than the substrate. In traditional molding processes, such as injection molding, release coatings are common. Mold release coatings also help to reduce mold wear and increase tooling life. The mold release agents can also increase the repeatability of the molding process. Several mold release agents were tested on aluminum stampers of different geometries and the release force from the different materials were measured.

Additionally, alternate stamper materials, particularly polymers, were used to attempt to facilitate release. Polymers were investigated rigorously in response to the

following statement made in the discussion section of Sohn and Dow [37], who were also investigating the use of the process to correct PMMA optics (emphasis added).

“Experiments with PMMA substrates were largely unsuccessful *because of poor bonding between PMMA and the epoxy* as well as difficulty in curing the epoxy through the plastic material since most commercial grades of PMMA are treated with a UV absorber.” The failure of the Summer Optic J-91 polymer to bond to PMMA substrates as noted by Sohn and Dow [37] fortuitously led us to investigate PMMA and other polymers as stamper materials.

### 3.2 Equipment Used

The force measurement tests used Summers Optical J-91 Lens Bond UV-Polymer as previously described. The release force experiments were conducted using the Kistler 3-axis dynamometer and charge amplifier. The dynamometer and charge amplifier used are shown in Figure 3.1. The dynamometer and amplifier could measure forces at +/- 250 N with a resolution of 2 mN.

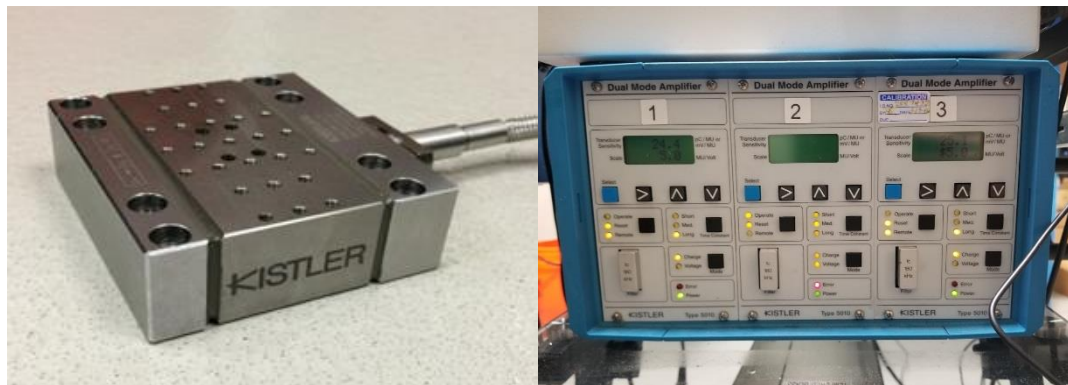


Figure 3.1 Kistler 3-axis dynamometer 9256C1 (left) and the charge amplifier (right)

The charge amplifier signal was collected using a National Instruments USB-6251 data acquisition (DAQ board) unit. The DAQ board was interfaced with a LabVIEW

program to display the force data as a live graph and to save the data. The data was collected at 5 kHz, which is approximately twice the natural frequency of the dynamometer with the mass of the experimental set up mounted on it. Thus, the dynamometer itself provided a mechanical anti-aliasing filter in the experiments. The National Instruments DAQ board is shown in Figure 3.2.

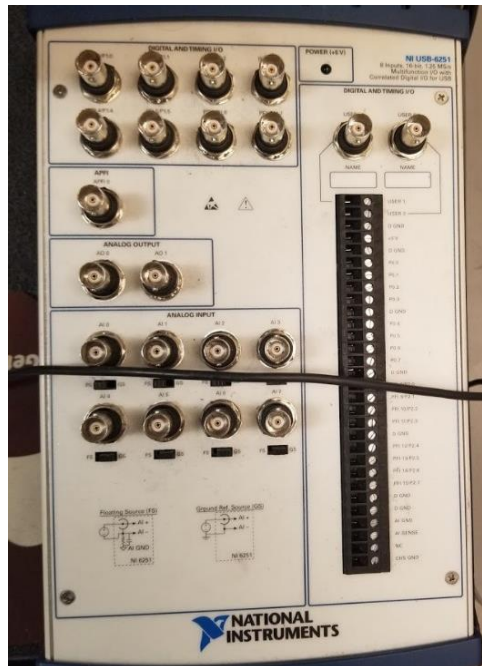


Figure 3.2 National Instruments USB-6251 DAQ board

The data acquisition was triggered from a switch that generated a signal from an Arduino Uno. The Arduino was used to drive a DC motor discussed below as well to trigger the data acquisition to begin. The Arduino had a motor shield mounted on it to drive the DC motor. The Arduino and the motor shield are shown in Figure 3.3.

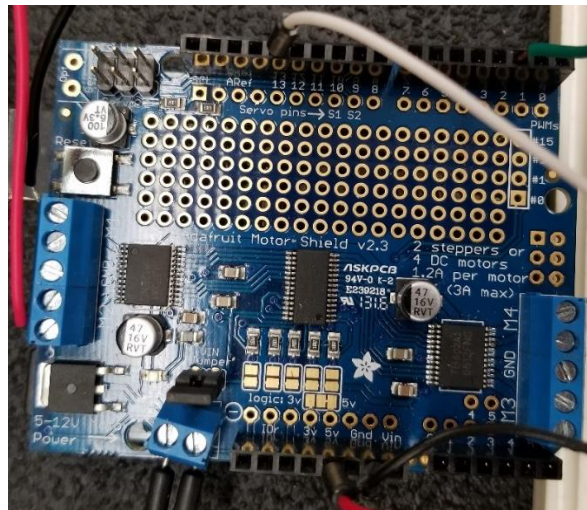


Figure 3.3 Arduino Uno with Adafruit motor shield

The DC motor was attached to a gear box with a gear reduction of 8:1 as shown in Figure 3.4. The motor and gear box were mounted to an aluminum bracket that has machined slots allowing the motor height to be adjusted. The motor height also determines the maximum position of the cam as discussed below. The bracket has mounting holes to allow it to be fixed to the same plate as the dynamometer which will be discussed in the experimental set up. The bracket was machined out of a single block of aluminum for rigidity.

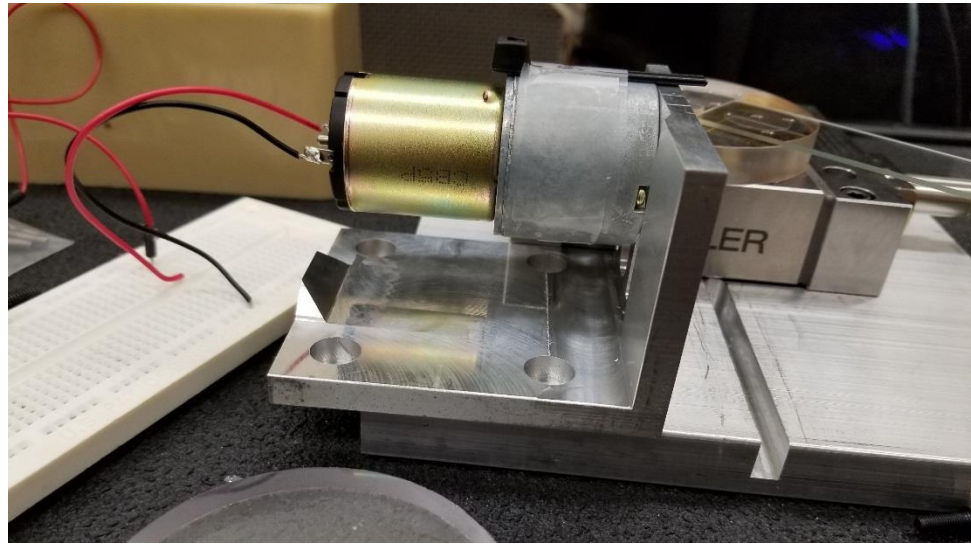


Figure 3.4 Geared DC motor and aluminum motor mount

An eccentric cam (Figure 3.5) was mounted on the motor shaft to produce a force on the test specimen and generate release. The gearbox reduced the speed of the motor and increased the torque/force that can be exerted during a relatively slow and controlled release process. The eccentric cam is a  $5/8^{\text{th}}$  inch diameter piece of mild steel with a hole drilled  $1/8^{\text{th}}$  of an inch off center. The cam is mounted to the shaft of the DC motor with a set screw.

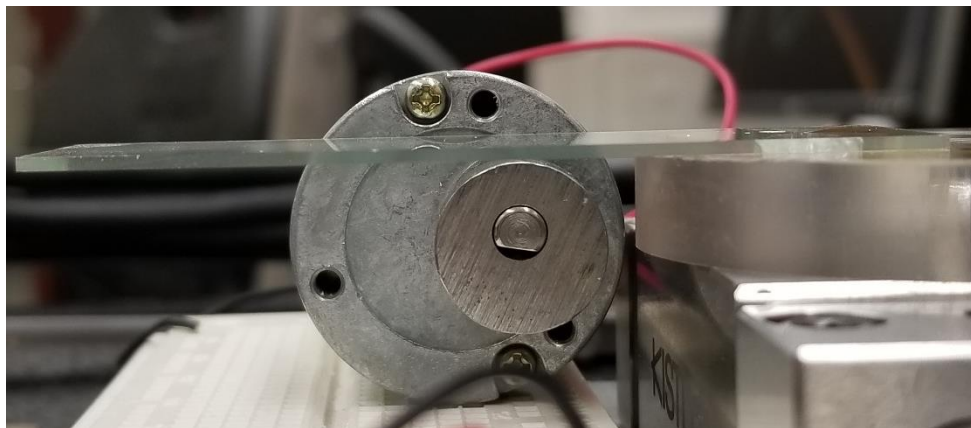


Figure 3.5 Eccentric cam actuator on DC moto

The replications were cured in the ELC-500 Light Exposure System by Electro-Lite Corporation. The exposure intensity was constant, and the cure time was varied. The curing chamber is shown in Figure 3.6.



Figure 3.6 The ELC-500 Light Exposure System by Electro-Lite Corporation.

### 3.3 Experimental Set Up

The force measurement experiments were set up to measure the force required to release a glass microscope slide (substrate material) adhered to a puck of test stamper material by the UV polymer. The materials used for the test pucks were aluminum, Poly (methyl methacrylate) (PMMA), and Teflon. Aluminum was chosen for force tests due to its good diamond turning behavior, the preliminary release tests and the suggestion of Sohn and Dow [37]. PMMA was chosen due to the quote in Sohn and Dow discussed above. Although not as good as aluminum, PMMA is also suitable for diamond turning under well-chosen conditions. The last material that was selected for testing was PTFE due to its low surface energy. As discussed above the low surface energy of PTFE (~19

mJ/m<sup>2</sup>) reduces its wettability compared to glass and thus makes release from the stamper and the polymer more likely than release from the substrate.

The materials were cut to test pucks 63.5 mm diameter and 12 mm thick. The pucks were drilled, counter sunk, and mounted to the dynamometer using an M2 screw. The aluminum samples were tested with a ‘rough machined’ surface finish (Sa of approximately 350 nm) and with a diamond turned surface finish (Sa of approximately 6nm). The dynamometer was mounted to an aluminum baseplate using the 10-32 hardware and mounting holes in the dynamometer. The geared DC motor and motor mount were also mounted to the base plate. A switch was used to turn on the motor and to trigger the LabVIEW program to start collecting the force data. The experimental set up can be seen in Figure 3.7.

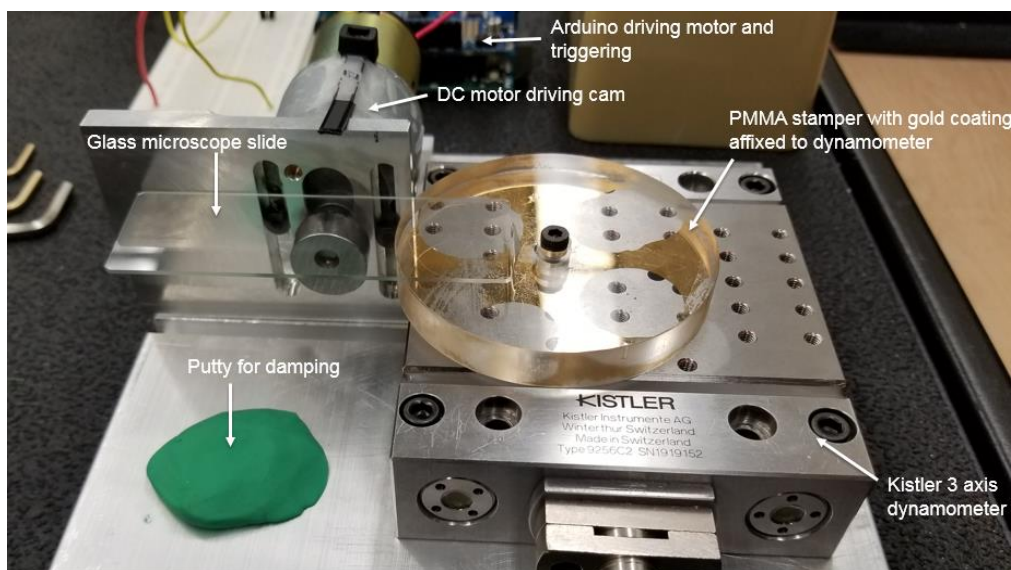


Figure 3.7 Force measurement set up

The motor height was set so that the maximum height of the cam would not extend beyond the thickness of the glass slide that was used. This ensured that the

maximum possible deflection of the glass was no more than the thickness of the glass slide. The distance from the motor shaft to the edge of the dynamometer was held constant and was approximately 19 mm away from the edge of the dynamometer. The slides were aligned against the side of the aluminum motor mount and were positioned as close to the mounting hole on the puck as possible. The pucks were then marked with masking tape to ensure that the slides were placed in the same location for each test. Two slides could be cured onto the puck at the same time so that multiple tests could be run with one curing cycle. An example of a PMMA puck is shown in Figure 3.8.

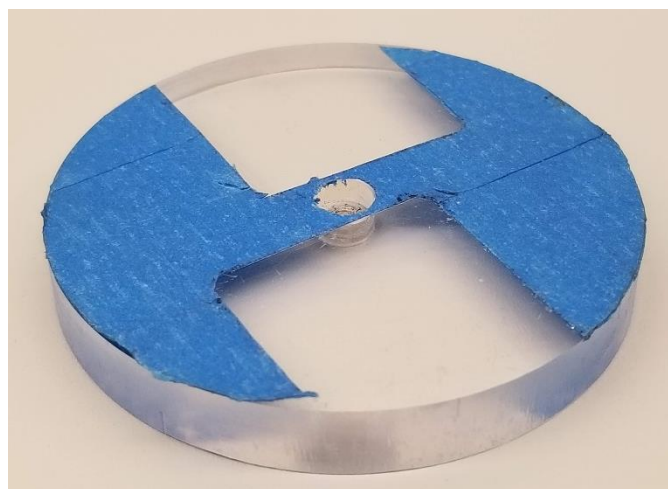


Figure 3.8 PMMA puck with masked areas for slides

The UV polymer was applied to the stamper by applying one drop from the dropper bottle. The drop was placed in the center of the area where the glass slide was to be applied. Once the polymer was applied, a glass slide was placed on top of the drop and the assembly was cured. After curing the puck was bolted to the dynamometer. The cure time was analyzed for PMMA and PTFE and will be discussed in the results. Release tests were considered a success if the polymer released from the puck and stayed fully

adhered to the slide. Tests were considered failures if the replicant did not stick to the glass slide or if the replication partially peeled away from the glass slide. The test was also considered a failure if the glass slide was broken during the process.

The initial experiments were conducted to compare Aluminum and PMMA. The aluminum sample was used to determine a baseline since as described in the previous chapter initial replication experiments were conducted with aluminum stampers. The results from these experiments are discussed below.

### 3.3.1 Sputtered Gold

The first mold release agent tested was sputtered gold applied with a sputter coater intended for use on SEM samples. The UV-polymer when cured is transparent and requires a reflective coating for operation. The tests were conducted to determine if the sputtered gold could be applied to the stamper and transferred to the cured replicant. Initial tests were conducted on the diamond turned aluminum puck with 50 nm of gold. The replicated flat and stamper are shown in Figure 3.9 below.

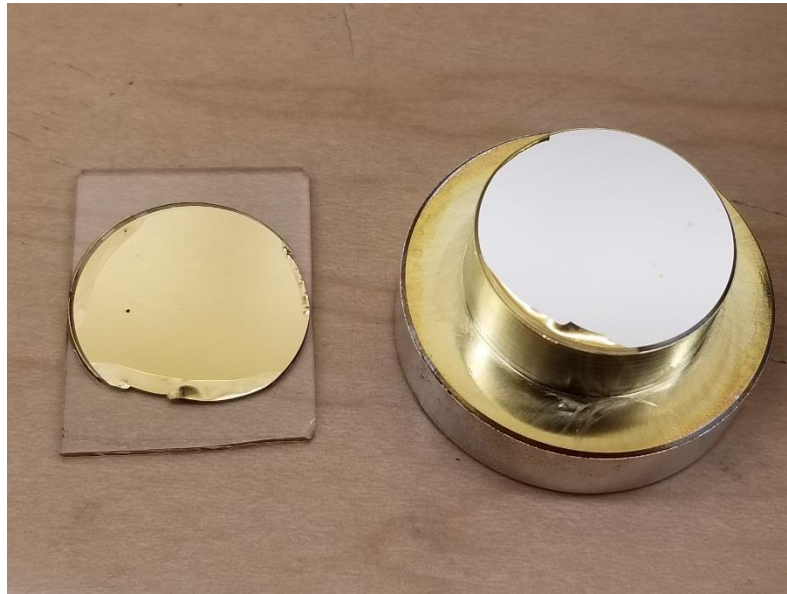


Figure 3.9 Aluminum flat sputtered with 50nm of gold

The gold adhered to the replicant and to the aluminum stamper. The replicant had pulled up edges and the gold showed lines where the replicant partially released. The replicated flat is shown in Figure 3.10. The 50 nm gold test showed that the reflective coating could be transferred with the replication and reduced the adhesion force between the replicant and the mold. The replication in Figure 3.10 shows the surface stress in the replicant and a partial release line. The next set of experiments used a thinner coating of gold to try to determine what thickness was most suitable as a release agent.

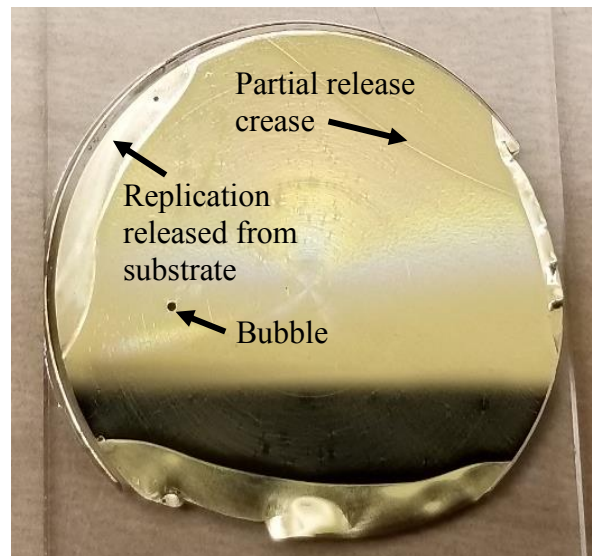


Figure 3.10 Replicated flat with 50nm of Gold

The next experiment was conducted using 25 nm of gold on the aluminum. This allowed the gold to be tested on the replication system and determine if the coating was able to increase the repeatability of the set up. The aluminum flat and replication are shown in Figure 3.11. The 25 nm gold coating did not reduce the force required to release the replicant from the mold and instead the substrate released from the substrate holder.

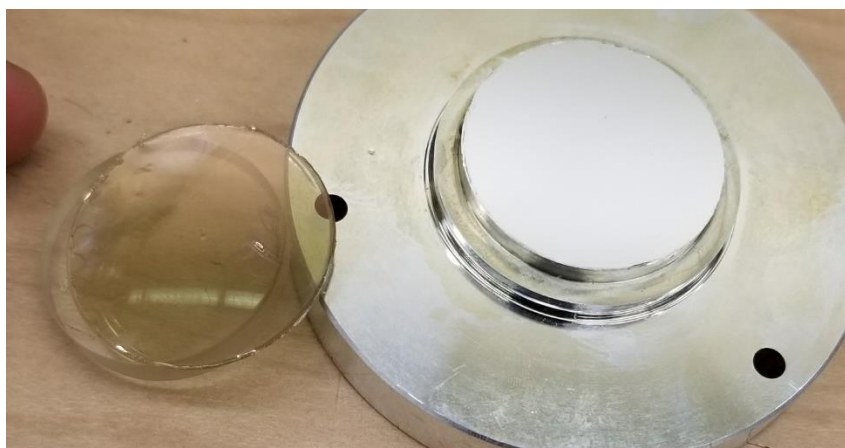


Figure 3.11 Aluminum flat sputtered with 25nm of Gold

The adhesion between the replication and the stamper was so great that the glass substrate partially released from both the stamper and the glass substrate. This result led to further examine other types of release agents. Based on the experience of Dr. Suleski, Aquaphobe CM was used as a release agent. The results of the Aquaphobe CM were inconclusive.

#### 3.4 Measurement Analysis and Results

The measurements from these experiments result in force data in the x, y, and z directions versus time. The data of interest is the z-direction. The z-direction describes the force to release the sample in the direction normal to the surface. The cam system and glass slide act as a lever and create a force vector that is a combination of x and z forces. The shearing force data in the x-direction could be analyzed for a more comprehensive understanding of the release mechanics associated with the glass slides, however for the purposes of comparing material combinations for the current replication system the z-forces were used. An example of a force measurement can be seen in Figure 3.12 below.

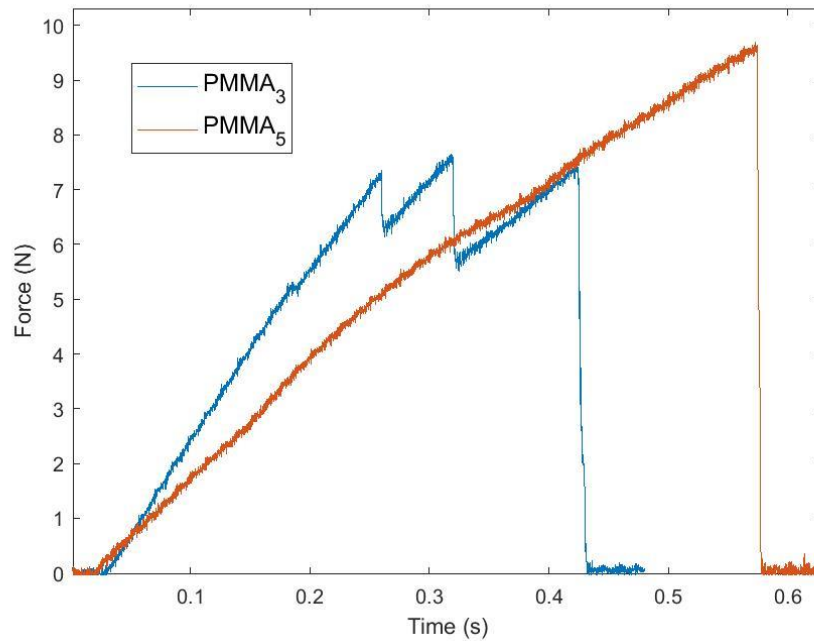


Figure 3.12 Force measurement from PMMA with and without partial release

The force data was imported into MATLAB and filtered using a low pass filter to reduce noise in the measurement. The cutoff frequency was set to 500 Hz. The data for PMMA, sample 5, linearly increases until 0.6 seconds and then the force rapidly decreases on release. The force graph of another PMMA sample (designated sample 3) shows two partial release zones before the replicant fully released from the puck. Partial release is evident in the rapid force drops that do not go to zero. This shows that the replicant is starting to peel away from the puck but does not fully release across the entire area. After partial release, the force begins to increase again until full release is achieved. This can happen several times before the replication fully releases. Partial releases are not favorable as they are typically associated with crease-like defects in the replica. During a

partial release some area of the replication has released while there is another area that is still adhered to the puck.

It was hypothesized that cure time might affect the tendency for partial release. Thus, experiments were conducted for various cure times. The cure time tests were conducted using the PTFE puck. The cure tests were done at 6, 9, and 18-minute cure times. The force measurements for the cure time testing can be seen in Figure 3.13 below.

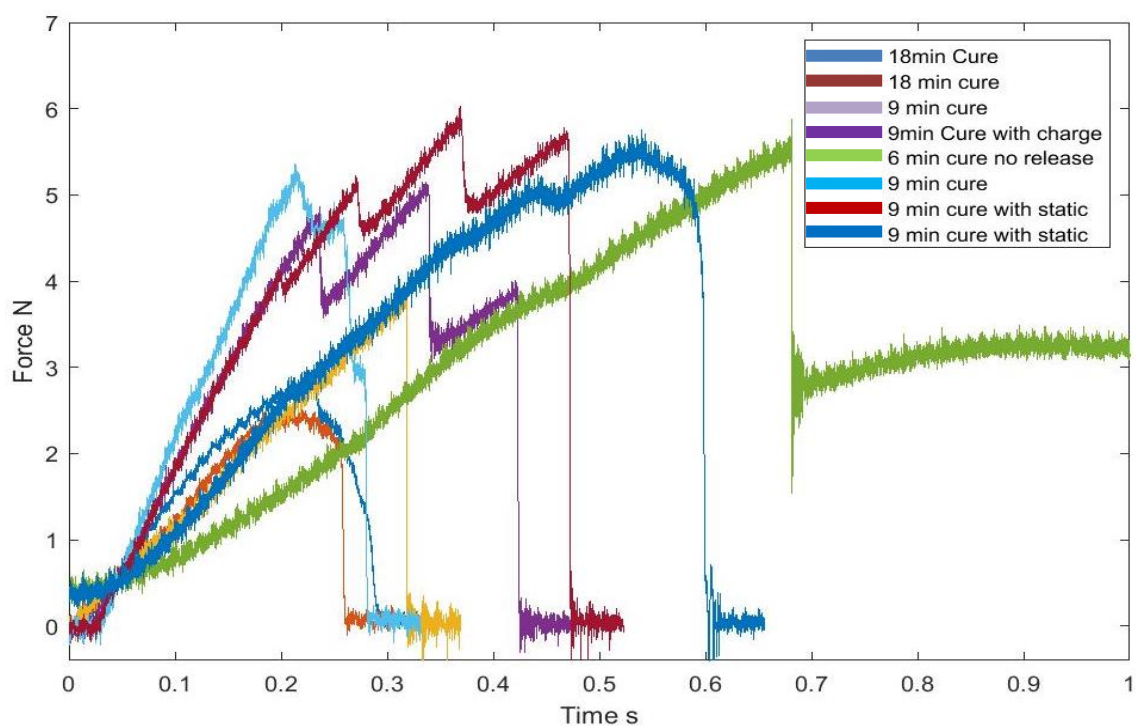


Figure 3.13 Force measurements for Teflon at different cure times

The force measurements in Figure 3.13 show that at 6 minutes the UV-polymer is soft, and the release takes more than the 1 second test time shown. Under these conditions the polymer was observed to deform significantly during partial release. The 9-minute cure time measurements show partial release in 4 out of the 5 measurements. The 18-minute cure time reduced the maximum release force and made the release more

consistent. The cure time experiments showed that at 9 minutes the UV-polymer was not fully cured. The cure time was extended for future experiments to ensure a fully cured replicant.

The force measurements were used to determine the best of the material combinations to reduce the release force during the replication process to increase the repeatability. After the force measurements were conducted and the cure time was examined, the maximum force for each experiment was plotted versus the candidate stamper material. The maximum force values for 16 force measurement experiments can be seen in Figure 3.14.

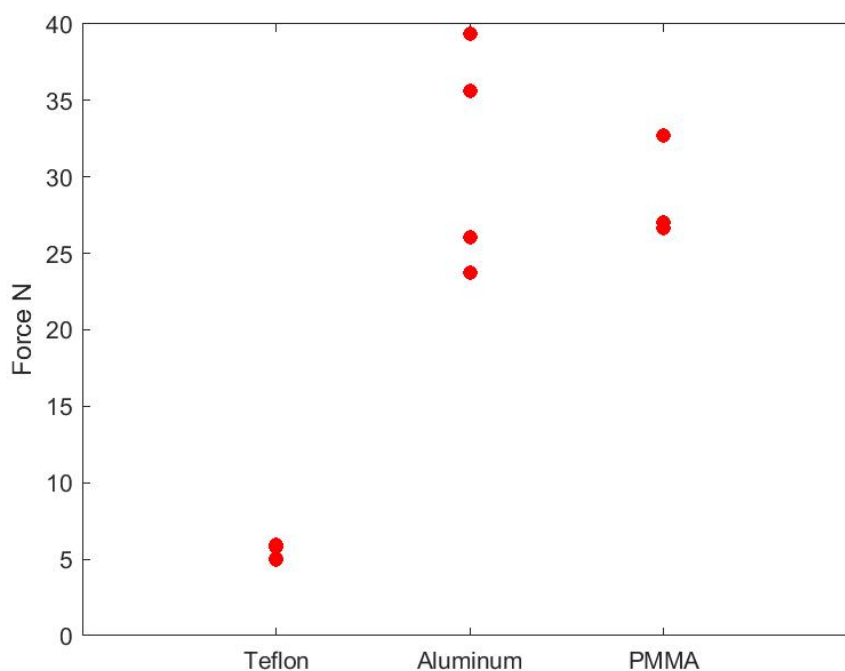


Figure 3.14 Maximum force from measurements of Teflon, aluminum, and PMMA

The maximum force values for PTFE were lower than any values of PMMA and aluminum and were more consistent. These experiments indicated that based on release

forces and repeatability, PTFE was the best choice for the stamper material. However, the diamond turnability of PTFE had to be assessed to determine its suitability as a stamper material.

## CHAPTER 4: SURFACE ROUGHNESS OF DIAMOND TURNED TEFLON

### 4.1 Introduction

The effect of cutting parameters on the surface roughness of diamond turned polytetrafluoroethylene (PTFE) was examined. Next the surface roughness of ultra-violet (UV) cured polymer freeform corrective surfaces are compared to the surface of diamond turned PTFE molds.

It is well known that ultra-violet curable polymers are ideal for replication of surface features down to the sub-micrometer and even nanometer level with high fidelity. It was shown that replications of diamond turned PTFE samples can replicate the surface features to a high degree. PTFE is used in many applications for its high lubricity and is used here as a stamper material due to its tendency to release easily from the molded polymer at low force levels. As described in Chapter 1, multi-axis diamond machining has been used for the direct machining of freeform optics and is thus a suitable process for machining the freeform stampers. However, due to the tribo-chemical interactions between the tool and workpiece, only certain materials can be turned with a diamond tool optical level surface finish and minimal tool wear. PTFE is highly inert material that should not cause chemical wear of diamonds. In diamond machining materials that do not cause significant tool wear, the roughness of the surface generated by a round nosed tool is dominated by the geometric properties of the cusp structures generated as the tool moves over the surface. Under these simple conditions the minimum theoretical surface roughness obtained is proportional to the square of the feed motion per revolution of the workpiece and is inversely proportional to the radius of the tool. Under such ideal

conditions, the feed rate and tool radius can be selected to achieve a desired surface roughness. However, for polymer materials such as PTFE the cutting mechanics can also significantly affect the roughness and the simple geometric model for surface roughness breaks down. The roughness then depends on other cutting parameters such as depth of cut, rake angle and cutting speed. Under these conditions, more extensive empirical experiments and/or simulation are required to achieve desired surface roughness and indeed in complex materials such as PTFE it may not be possible to achieve the desired surface roughness. As will be shown below, for PTFE there appears to be a surface roughness limit that depends on cutting speed. Further, that chip evacuation is a large factor in diamond turning of PTFE. Chip buildup can cause the PTFE to plastically deform leaving gouges or tears in the surface.

#### 4.2 Experimental Setup

The value of surface roughness was compared to the theoretical by conducting cutting experiments with different feed rates. A 63.5mm diameter 8 mm thick PTFE sample was used in the experiments. The sample was divided into 9 bands that were each 0.5 mm wide with each band cut at a different feed rate. The experiments were repeated for two cutting speeds 0.3 m/s and 3 m/s. Since the radius of the bands changed during the tests, the spindle speed had to be adjusted according to Equation 4.1 for each band.

$$RPM = \frac{\text{Desired Cutting Speed} \left(\frac{m}{s}\right) * 10^{-3}}{2 * \pi * \text{Average radius}(mm)} * 60 \frac{s}{min} \quad \text{Equation 4.1}$$

The average radius for the band was defined as the average of the maximum and minimum radii bounding the band. The feed rates and spindle speeds used for each band are given in Table 4.1.

Table 4.1 Feed rates and spindle speed for the two chosen cutting velocities.

3 (m/s)		.3 (m/s)	
f ( $\mu\text{m}/\text{rev}$ )	RPM	f ( $\mu\text{m}/\text{rev}$ )	RPM
0.1	1139	0.1	114
0.3	1186	0.3	119
1	1238	1	124
2	1294	2	129
5	1355	5	135
10	1422	10	142
20	1496	20	150
30	1579	30	158
40	1671	40	167

The feed rates chosen for this experiment range from aggressive roughing feeds down to finishing feed rates. The diamond tool that was used in this experiment had a tool nose radius of 250  $\mu\text{m}$  and a zero-rake angle. The tool was mounted on a tool post and set up for facing. The part was held on the spindle with a vacuum chuck and faced before cutting the bands at the two cutting speeds. The 0.5 mm bands start at a radius of 25.4 mm and end at a radius of 13.9 mm. The sample that was used for the cutting tests is shown in in Figure 4.1. A set of bands can be seen between the two arrows in the image.

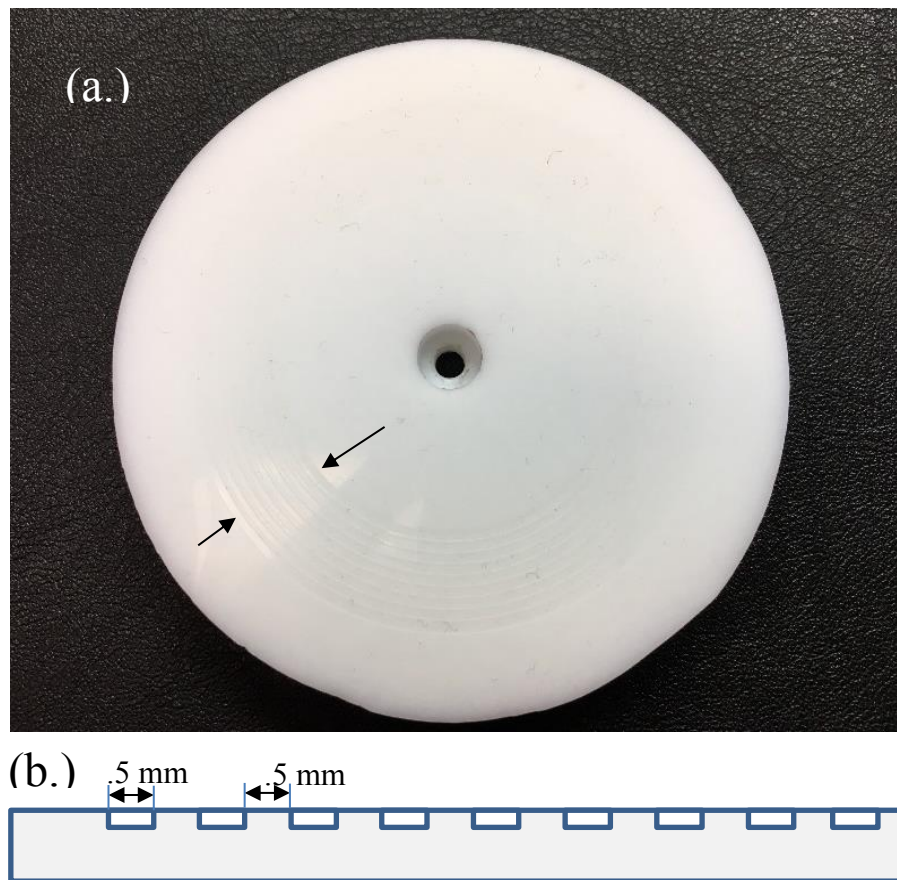


Figure 4.1 (a.) Teflon sample (b.) cross section showing 9 different 0.5 mm radial bands between the arrows

Two different depths of cut were used for each cutting velocity, 25  $\mu\text{m}$  and 50  $\mu\text{m}$ . Thus, four sets of eight tests were completed in all. The 25  $\mu\text{m}$  depth of cut is a typical depth of cut for rough passes in diamond turnable materials and the 50  $\mu\text{m}$  depth of cut was chosen to evaluate how PTFE would respond under more aggressive conditions. Initial tests were completed at 50  $\mu\text{m}$  to ensure that the forces were not high enough to cause the part to release from the vacuum chuck.

During preliminary cutting tests, it was observed that if mineral spirits were used as a lubricant, the chips would stick to and damage the surface. Thus, only pressurized air was used to evacuate the chips. The air jets were set to blow the chips away from the

newly cut surface by positioning one jet just below the cutting edge of the tool blowing upward and placing the second jet to blow the chips away from the newly cut surface across the top of the cutting tool. It was also observed that the chips were highly charged when coming off the part and would adhere to nearby objects due to static charge. Experiments were not conducted to attempt to measure or observe the buildup of charge during cutting.

After each set of eight bands were machined the surface roughness was measured using the Zygo Nexview coherence scanning interferometer (CSI). The 50x objective was used for these measurements. This produces a 168  $\mu\text{m}$  square field of view. The data was processed using Zygo Mx. The data was processed with band pass filter having a wavelength cutoff at 80  $\mu\text{m}$  and 2.5  $\mu\text{m}$  as specified by ISO 10110 part 8, section 4.3.2, “RMS roughness and RMS waviness” and in ISO 25178 part 3 section 4.4. Plane and tilt were also removed from the surface data before processing. Once the data was filtered, 10 profiles were calculated perpendicular to the cutting direction. These profiles were used to calculate the arithmetic average ( $R_a$ ) of the surface to compare it to the theoretical  $R_a$  of a diamond turned surface.

Diamond turned surface profiles can be modeled as a periodic cusp structure. The cusps are generated by the radius of the diamond tool and the stepover of the tool during turning. This has been well understood and modeled as discussed above and the theoretical cusp structure of a profile can be seen in Figure 4.2 after Qu and Shih [34].

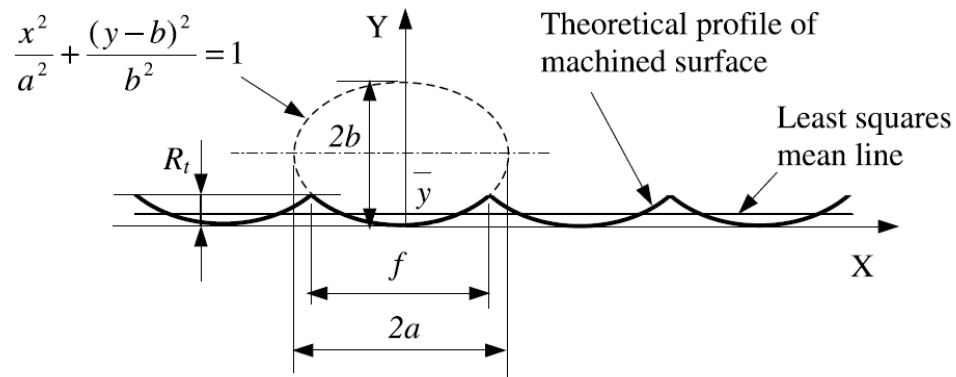


Figure 4.2 Diamond turned surface profile modeled as elliptical arcs

This model is for elliptical arcs which can account for non-zero rake angle tools. For  $a = b = R$  where  $R$  is the tool nose radius the cusp pattern is circular as is obtained with a zero-rake angle tool. The feed per rev is  $f$ . For this situation, the  $R_a$  can be analytically calculated and is given by Equation 4.2.

$$R_a \cong \frac{f^2}{9\sqrt{12}R} \quad \text{Equation 4.2}$$

This approximation holds true for  $\frac{f}{R} \ll 1$ . Equation 4.2 was used to calculate the approximate  $R_a$  value for the feed rates. The theoretical value was compared to an average  $R_a$  calculated from 10 profiles perpendicular to the cutting direction. The location of the profiles on the CSI measurement is shown in Figure 4.3.

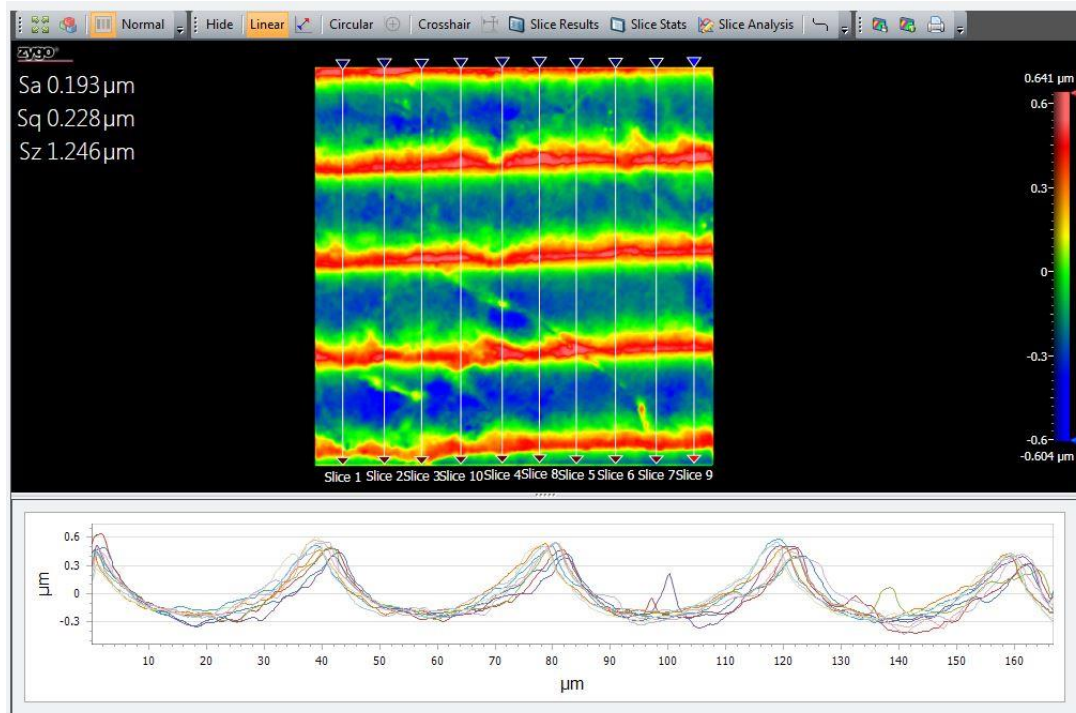


Figure 4.3 Areal data with 10 profiles used to calculate the average Ra of the surface

It can be seen in Figure 4.3 that the cusps are not perfectly horizontal due to the change in peak position in the profile plot. Data was corrected if the cutting direction was outside approximately 2 degrees from horizontal. Once the measurement was set up, the processing statistics tab was used to generate the selected parameters for all the profile data. The values calculated for one of the experiments generated using the processing statistics can be seen in

Table 4.2.

Table 4.2 Values generated using the processing statistics function of Mx

V <sub>ct</sub> = 0.3 m/s, 25 μm DoC, R = 250 μm												
Band	rpm	Sa (nm)	Sq (nm)	Sz (nm)	Sku	Ssk	Sal (μm)	Std (°)	Str	Ra_avg (nm)	Ra_est (nm)	
f1	0.1	114	49.994	62.123	362.012	2.76	-0.43	5.994	92.459	0.21	52.53	0.001
f2	0.3	119	75.649	89.991	835.121	2.82	-0.31	5.013	102.536	0.33	74.74	0.012
f3	1	124	62.059	77.116	474.412	2.62	-0.36	4.398	99.434	0.22	72.91	0.128
f4	2	129	55.024	68.543	589.958	2.84	-0.07	4.541	105.813	0.46	69.98	0.513
f5	5	135	61.508	75.386	544.391	2.22	-0.24	2.986	105.600	0.19	79.85	3.208
f6	10	142	61.395	75.394	521.713	1.97	-0.12	3.188	90.137	0.04	117.48	12.830
f7	20	150	55.742	69.075	482.885	3.21	1.06	6.029	90.019	0.07	114.76	51.320
f8	30	158	184.304	230.633	1417.424	1.77	0.24	4.159	90.010	0.05	104.85	115.470
f9	40	167	127.733	151.414	817.620	2.31	0.47	8.009	90.023	0.10	191.81	205.280

The values for Ra for each of the profiles were averaged and included in Table 4.2. It can be seen that at the higher feed rates, the estimated and measured Ra values agree fairly well, but significant deviation is seen for the lower feed rates. Agreement for high feed rates is expected for these conditions as exemplified in Figure 4.3 where a well-defined circular cusp pattern is evident. For lower feed rates the cusp pattern is not so evident and significant deviations are seen.

The surface texture direction (Std) gives the angular direction of absolute maximum of the angular spectrum as defined by ISO 25178-part 2 section 4.5.1. This value was helpful in aligning the data so that the cutting direction was aligned with the horizontal axis for each measurement.

The average Ra was calculated for each of the four experiments and compared to the theoretical Ra value.

The goal of these experiments was to identify optimal cutting parameters to achieve the desired surface finish in PTFE during diamond turning for production of optical molds for replication.

#### 4.3 Results and Discussion

The Ra parameter was chosen for comparison because it is common to calculate the approximated Ra value for the theoretical model of a diamond turned surface as discussed above. This is a good approximation used when turning to determine the necessary feed to achieve a desired surface roughness although it is not a robust surface parameter. The value for the Ra for the theoretical surface decreases in proportion to the square of the feed rate as described in Equation 4.2. The measurements of the PTFE show that this is only true for feed rates greater than 20  $\mu\text{m}/\text{rev}$ . The average Ra from

Table 4.2 and the theoretical Ra value calculated were plotted along with the average Ra values for the other two cutting tests. Figure 4.4 shows a comparison of the theoretical Ra and the experimental results for the different tests.

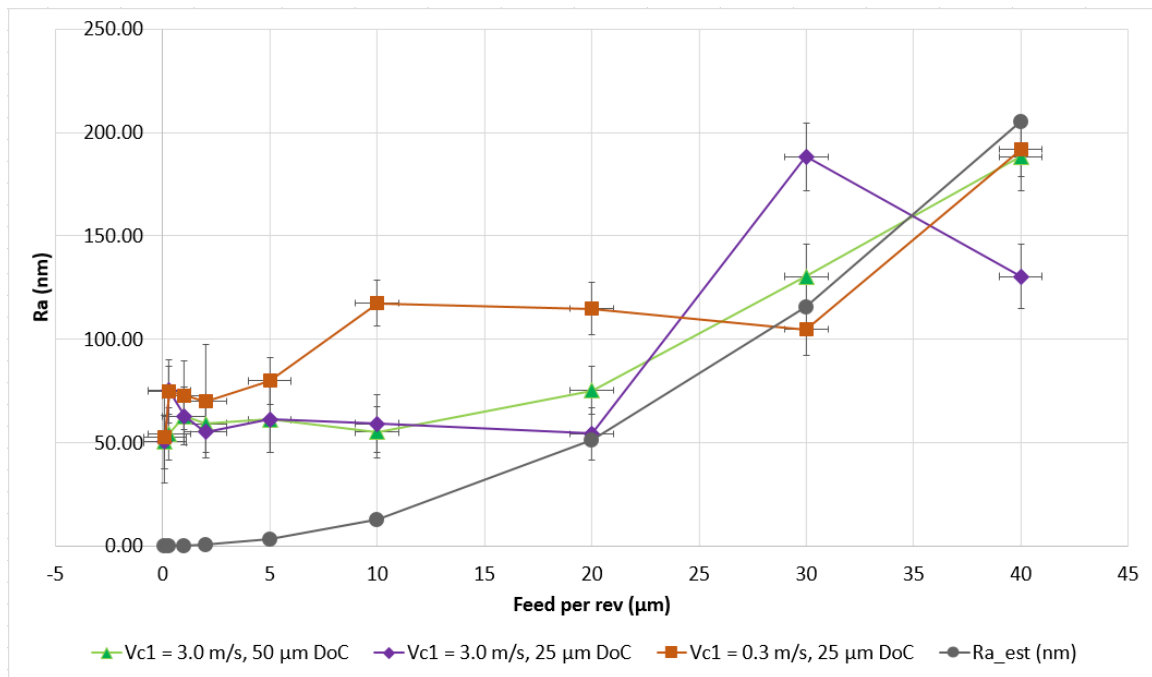


Figure 4.4 Theoretical and measured  $Ra$  for three cutting tests with different cutting parameters

The connecting lines in Figure 4.4 only serve to differentiate the four different data sets. The data shows a lower limit of  $Ra$  around 50 nm. The data shows a correlation with the theoretical at feed rates above 20  $\mu\text{m}/\text{rev}$  but for feed rates below 20  $\mu\text{m}/\text{rev}$  there is a limit to the minimum achievable surface roughness. Materials that diamond turn well such as copper, brass, germanium and (clean) aluminum follow the theoretical curve down to much lower surface roughness values of approximately 2 nm or slightly less. The causes for the disagreement were investigated further by looking at the power spectral density (PSD) functions calculated on traces perpendicular to the cutting direction.

A PSD characterizes the “power” in a signal or trace as a function of spatial frequency (or wavelength). Peaks in the PSD represent more dominant spatial

frequencies in a trace. For our measurements, the average PSD was calculated using all of the data sets in the y-direction, perpendicular to the cutting direction. The PSD of the cut done at 3 m/s, 25  $\mu\text{m}$  depth of cut and a feed rate of 40  $\mu\text{m}/\text{rev}$  is shown in Figure 4.5.

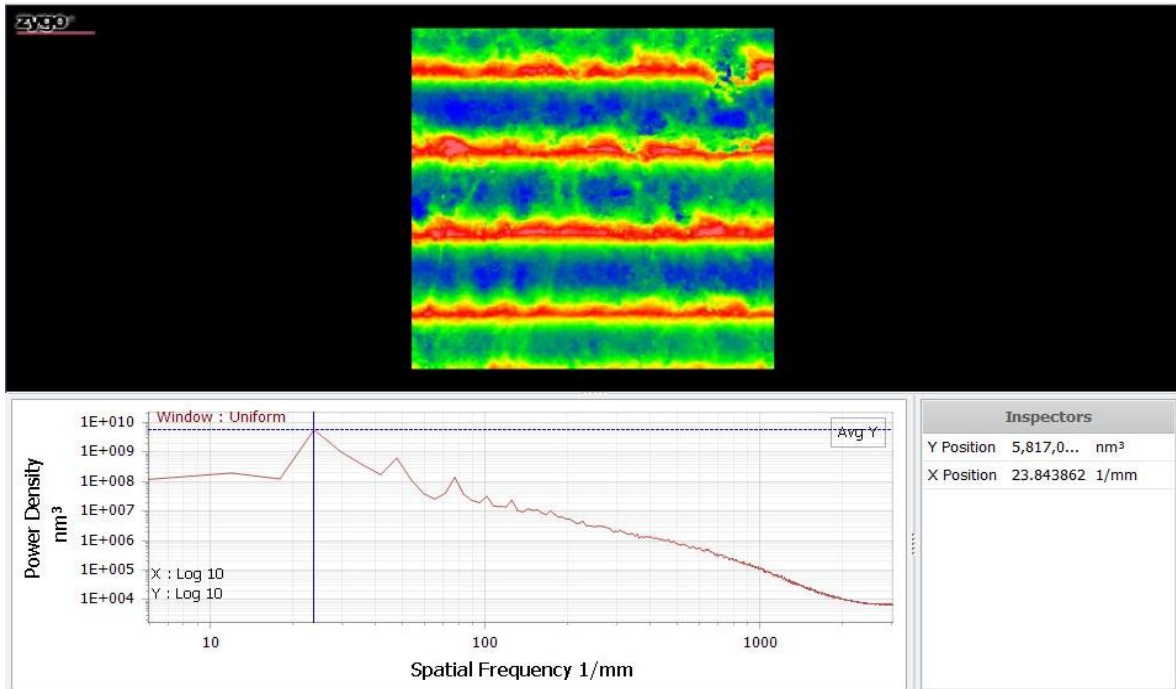


Figure 4.5 PSD of surface for cutting conditions:  $V_c = 3$  m/s, DoC = 25  $\mu\text{m}$  and 40  $\mu\text{m}/\text{rev}$

It can be seen in Figure 5 that there is a peak at a spatial frequency of 23.84 1/mm. Taking the reciprocal of the value gives a spatial wavelength of approximately 42  $\mu\text{m}$ . This is close to the feed rate for this band, 40  $\mu\text{m}$  per rev. However, because the field of view is only 168  $\mu\text{m}$  by 168  $\mu\text{m}$  only approximately four feed cycles can be resolved in the image. Thus, the peak is only roughly identified. If a larger field of view were used, the peak could be more precisely identified and should be 40  $\mu\text{m}$ . In diamond turnable materials the feed per rev is the dominant feature determining the roughness. While the feed per revolution is clearly evident in the image at 40  $\mu\text{m}$  per rev and at 20

$\mu\text{m}$  per rev it becomes less evident for  $5 \mu\text{m}$  per rev and is dominated by process effects at  $1 \mu\text{m}$  per rev. The PSD for several feed rates can be seen in Figure 4.6.

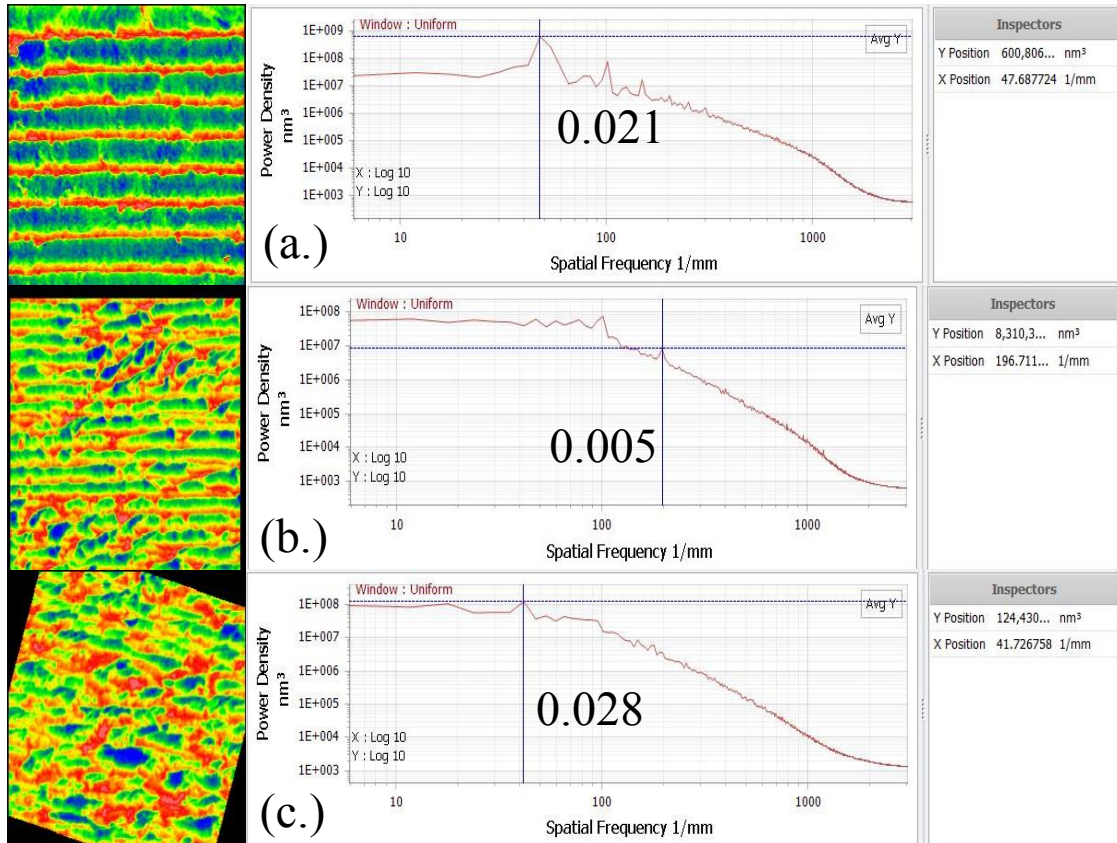


Figure 4.6 PSD of surface for cutting conditions:  $V_c = 3 \text{ m/s}$ ,  $\text{DoC} = 25 \mu\text{m}$  and (a.)  $20 \mu\text{m/rev}$  (b.)  $5 \mu\text{m/rev}$  (c.)  $1 \mu\text{m/rev}$

It can be seen that at  $20 \mu\text{m/rev}$  and at  $5 \mu\text{m/rev}$  more feed cycles can be seen and the PSD accurately shows the feed rate is a dominant frequency. In Figure 4.6 (b.) and (c.) the surface can be seen to start to degrade. The surface is no longer dominated by the cusp structure for Figure 4.6 (c.). The feed per rev at  $1 \mu\text{m}$  per rev is approaching the Nyquist limit of the detector. The feed per rev below  $1 \mu\text{m}$  per rev are below the Nyquist limit. The PSD was analyzed in the same manner for the three data sets and the spatial wavelengths were collected for each test and can be seen in

Table 3.

Table 3 Spatial wavelength from the PSD for the three data sets

	Vc=0.3 m/s, DOC = 25 $\mu\text{m}$	Vc=3 m/s, DOC = 25 $\mu\text{m}$	Vc=3 m/s, DOC = 50 $\mu\text{m}$
Feed ( $\mu\text{m}/\text{rev}$ )	Spatial wavelength (mm)	Spatial wavelength (mm)	Spatial wavelength (mm)
0.1	~	~	~
0.3	~	~	~
1	~0.028	~0.028	0.014
2	~0.008	~0.008	0.002
5	0.005	0.005	0.005
10	0.009	0.009	0.009
20	0.021	0.021	0.021
30	0.028	0.028	0.028
40	0.043	0.043	0.043

The peak spatial wavelengths correspond well with the feed down to approximately 1  $\mu\text{m}/\text{rev}$  and as discussed above the feed per rev drops below the Nyquist limit of the detector and the spatial wavelength cannot be detected. The cusp structure is further examined to evaluate the surface for the different cases. A profile was taken through the 3 m/s 25  $\mu\text{m}$  depth of cut sample at 40  $\mu\text{m}/\text{rev}$  and the cusp structure can be seen in Figure 4.7.

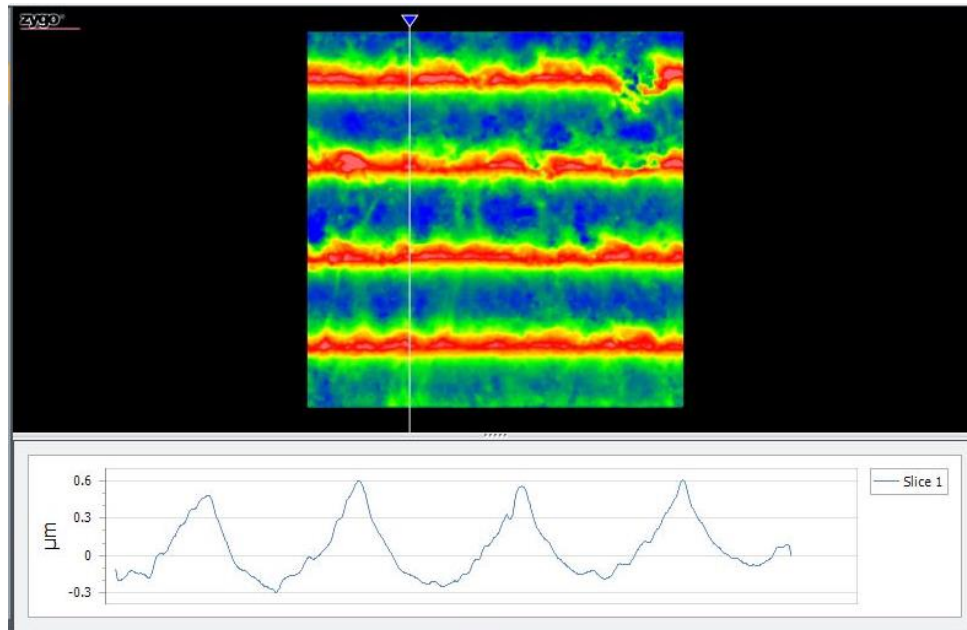


Figure 4.7 Profile of Teflon  $V_c = 3$  m/s, DoC =  $25 \mu\text{m}$  and  $40 \mu\text{m/rev}$

The profile in Figure 4.7 shows clearly the peaks and valleys but there are also smaller surface features that are irregular at shorter spatial wavelengths. These features are likely the reason that the surface roughness is limited to  $50 \text{ nm}$ . It appears that the PTFE material is not flowing off the surface uniformly. This could be due to the long chain molecules inherent in the structure of PTFE. In metals, ductile deformation occurs due to dislocation formation and material flow with a very small length scale. Perhaps because of the large molecule in PTFE the material flow has a larger characteristic length scales and this is evident in the surface. The phenomenon becomes more dominant at lower feed rates as the cusp structure in the direction perpendicular to the cutting direction begins to be dominated by the characteristics of the material flow in the cutting direction.

Figure 4.8 shows a surface measurement made with the 20x objective with a field of view of 417 by 417  $\mu\text{m}$  on a freeform stamper generated in coordinated axis turning mode with DoC=25  $\mu\text{m}$  and  $f = 25 \mu\text{m}/\text{rev}$ . The spindle speed was 100 rpm and the approximate radius at this location was  $R = 3 \text{ mm}$  giving a cutting speed of approximately  $V_c = .03 \text{ m/s}$ .

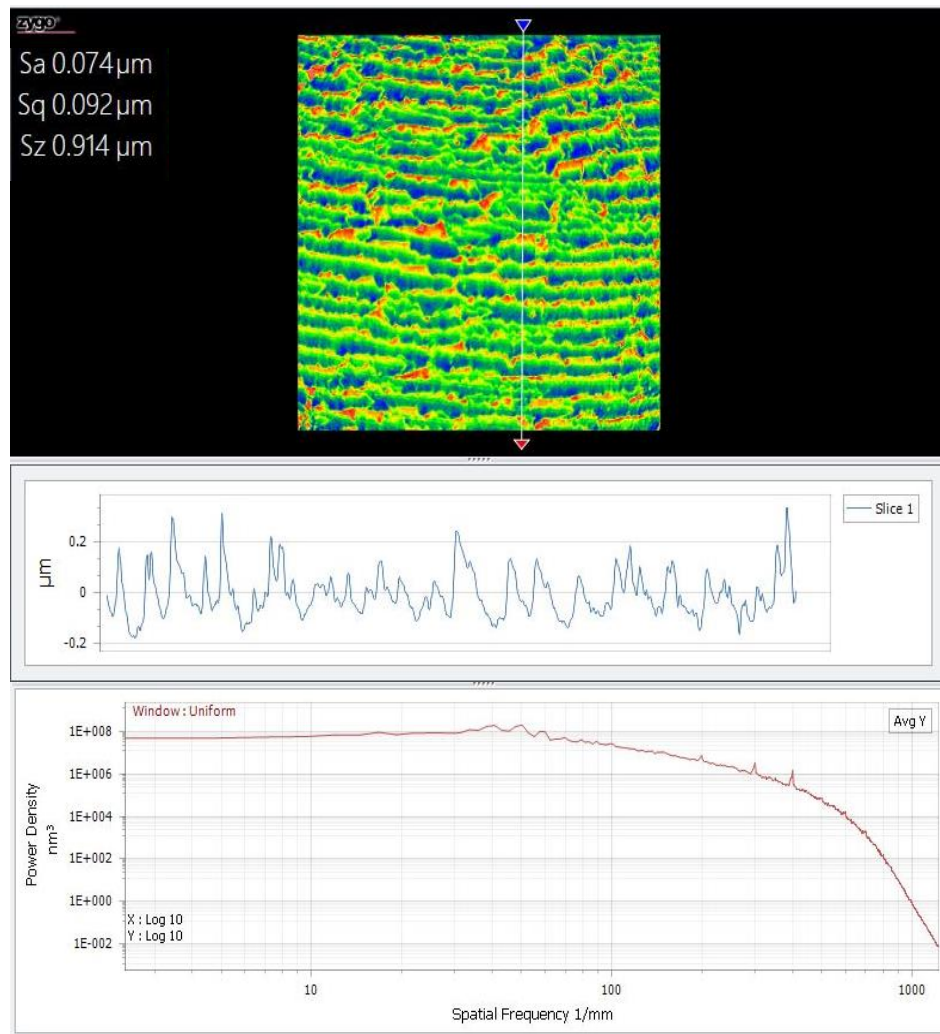


Figure 4.8 20x measurement of the Teflon stamper and average PSD of the profile with  $V_c = .03 \text{ m/s}$  DoC=25  $\mu\text{m}$  and  $f = 25 \mu\text{m}/\text{rev}$

While the feed rate is still evident in Figure 4.8, variations in the cutting direction presumably due to irregular material flow are becoming the more dominant features. The average PSD of the surface shows a small peak at 400 1/mm which does correspond to the feed rate of 2.5  $\mu\text{m}/\text{rev}$  as well as a peak at 200 1/mm and 300 1/mm. The Ra was not calculated for this profile however the areal equivalent of the arithmetic mean height Sa was calculated at 74 nm  $\pm$  7 nm. The areal RMS (Sq) was calculated at 92 nm  $\pm$  8 nm. It can be seen from the profile that there is no longer a clear cusp structure. While the feed is still visible in the areal data, it is not immediately evident in the individual traces. Irregular material removal is evident likely due to the large chain molecular structure of the material and perhaps the viscoelastic behavior. In a viscoelastic material, elastic deformation occurs nearly instantaneous upon loading whereas viscous effects such as relaxation will occur with a specific time scale. So perhaps fluctuations in the material flow could be the result of cycles of rapid elastic deformation followed by unloading over a longer time scale. Proving this hypothesis would require more experimentation and measurement of cutting forces that is beyond the scope of this work.

The replicated surface generated by the PTFE stamper shows the inverse of the surface features evident in the stamper in Figure 4.9.

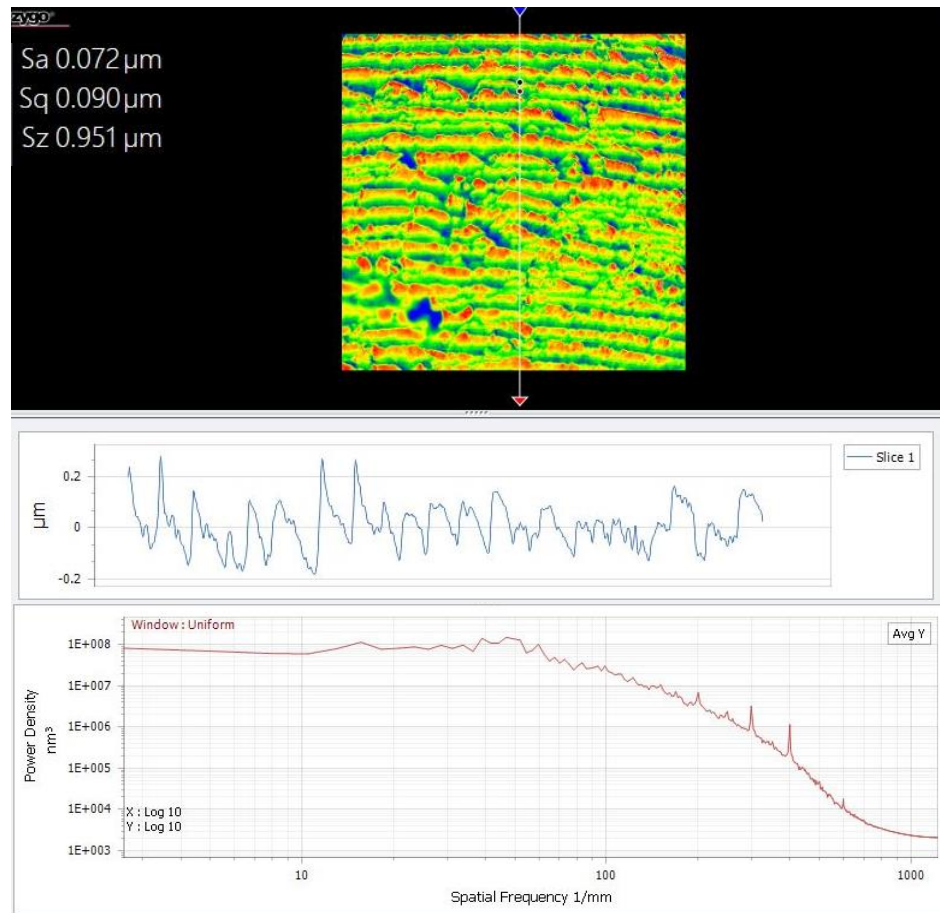


Figure 4.9 20x measurement of replication with profile and average PSD of the replication

The average PSD of the replication shows the same peak as the stamper at 400 1/mm, which corresponds to a federate of 2.5  $\mu\text{m}/\text{rev}$ , and peaks at 200 and 300 1/mm. The replication shows the very sharp peaks and valleys of the stamper. The stamper peaks were very sharp and narrow as well as the valleys and these features were replicated well.

#### 4.4 Conclusions and Future Work

PTFE may be a viable material for diamond turning and hence could be used for the stamper. However, to achieve suitable surface roughness more tests must be

conducted, and the cutting mechanics better understood. The cutting speed required for optical surfaces may be too high to operate the machine in coordinated axis mode. The replication process used is capable of replication of optical surfaces and this replicated the surface of the Teflon well. The power spectral density is a very useful tool to examine surfaces with periodic features and can show the feed rate that was used to cut a part.

To determine suitable cutting conditions for PTFE more cutting experiments need to be conducted to determine if the surface roughness can be reduced. Rake angle experiments should be conducted to determine the optimal setup for cutting PTFE. Diamond turning polymers produces large amounts of static charge and the effects were not examined in this work but would be helpful to better understand.

## CHAPTER 5: REPLICATION RESULTS

### 5.1 Introduction

The goal of this work is to replicate a freeform corrector on a glass substrate. Numerous issues have been researched and several conclusions have been drawn that bring us closer to the goal. An alignment system has been developed that controls the gap and centration, the two most important positioning tolerances in the replication process. While it does not produce the surface finish required for optics, PTFE has been identified as a material that can be diamond turned and can be used as a stamper that releases easily from the polymer leaving it bonded to the glass substrate. And PTFE impregnated nickel phosphorus seems to be a viable alternative material for the stamper that may produce optical surface finish and form while not adhering to the polymer correction layer. What remains is to test the capability of the process to repeatedly produce optical form in the polymer on the glass substrate. One major issue that still remains to be addressed is shrinkage of the polymer on curing. Sohn and Dow [37] identified this as a potential significant challenge, attributing form errors in the replicated surface to bending deformation in the substrate caused by residual stresses in the cured polymer layer. However Sohn and Dow [37] found a form error that seemed to indicate that the polymer was not shrinking during the curing process but rather expanding. This seemed an unlikely conclusion. Alternatively, what we have found in doing replications on mechanically robust substrates is that volumetric shrinkage of the polymer, producing on the order of 2% strain, directly leads to form errors in the optic. However, as we show here the shrinkage is repeatable and can be compensated by changes in the mold dimensions.

Further, because the freeform optic that we have targeted as one that can be replicated is very close ( $< 100 \mu\text{m}$ ) to a base sphere. Thus, the approach to correction that we have implemented is to (1) manufacture a stamper that matches the base sphere of the freeform optics; (2) replicate the sphere and measure the form errors in the sphere; (3) compensate the stamper to compensate the form errors in the base sphere; and (4) apply the same corrections to final freeform optic. As described here, we have accomplished three of these four goals, but final replication of the freeform and associated metrology, and additional correction if necessary, remains a topic for future research.

## 5.2 Shrinkage

Shrinkage in the replication process is to be expected and can be corrected for. The project was originally intended to replicate thin UV-polymer corrective layers on a base torus to replicate a freeform optic for the spectrometer primary optic described in Chapter 1. The repeatability of the replication process when the layers were sub  $100 \mu\text{m}$  was very poor due to adherence to the stamper and the alignment of a freeform stamper with a toroidal substrate introduced additional clocking tolerances in the replication system that did not have a high benefit and incurred a great deal of additional costs. Thus, the scope of the project changed from the replication of thin film UV-polymers ( $\sim 100 \mu\text{m}$ ) onto base toroidal substrates to the replication of thicker layers ( $300 \mu\text{m} - 600 \mu\text{m}$ ) and axisymmetric spherical substrates.

This shift in focus also allowed for the use of less expensive spherical glass rather than toroidal substrates. Such substrates are readily available at low cost as plano-convex or plano-concave spherical glass lenses. However, the use of thicker polymer layers led

to increased errors due to shrinkage. Following the work of Sohn and Dow [37] initial shrinkage characterization was done with the replications of cylindrical pillars/flats.

## 5.2 Equipment Used

Stampers suitable for replicating polymer cylindrical pillars were dubbed ‘top hat’ stampers. These were pre-machined on the HAAS TM-1 and then diamond turned on the Precitech Nanoform 350 shown in Figure 4.10.



Figure 4.10 Precitech 350 diamond turning machine

A Taylor Hobson Form Talysurf was used to take the profilometry measurements on the stampers and replications. The Moore Nanotech 350 FG was used to turn the spherical stampers. The curing chamber that was used was the ECL-500.

## 5.3 Shrinkage analysis using ‘top hat’ geometry

The initial shrinkage characterization was conducted with PMMA ‘top hat’ stampers. The ‘top hat’ geometry was selected to examine a replicated shape with a defined perimeter and a nominally flat top geometry. The stampers were designed to

examine the shrinkage over different thickness replications by changing the height of the cylindrical region to be replicated. Initially PMMA blanks were machined to the necessary geometry for use in the final replication system described in Chapter 3 as shown in Figure 2.9. The flange and outer diameter of the PMMA stampers were diamond turned to interface with the diamond turned spacer ring. Four PMMA stamper were machined that had different recess depths. The depths were: 25  $\mu\text{m}$ , 50  $\mu\text{m}$ , 100  $\mu\text{m}$ , and 150  $\mu\text{m}$ . The 25  $\mu\text{m}$  ‘top hat’ stamper is shown in Figure 4.11.

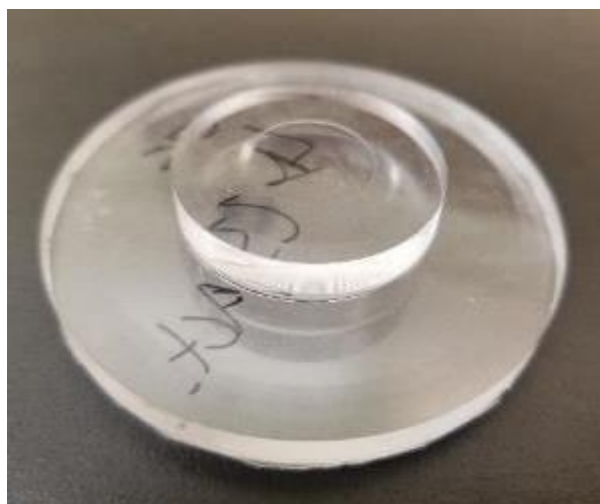


Figure 4.11 PMMA ‘top hat’ stamper with 25  $\mu\text{m}$  deep cylindrical recess.

A profilometer measurement for the 25  $\mu\text{m}$  stamper is shown in Figure 4.12.

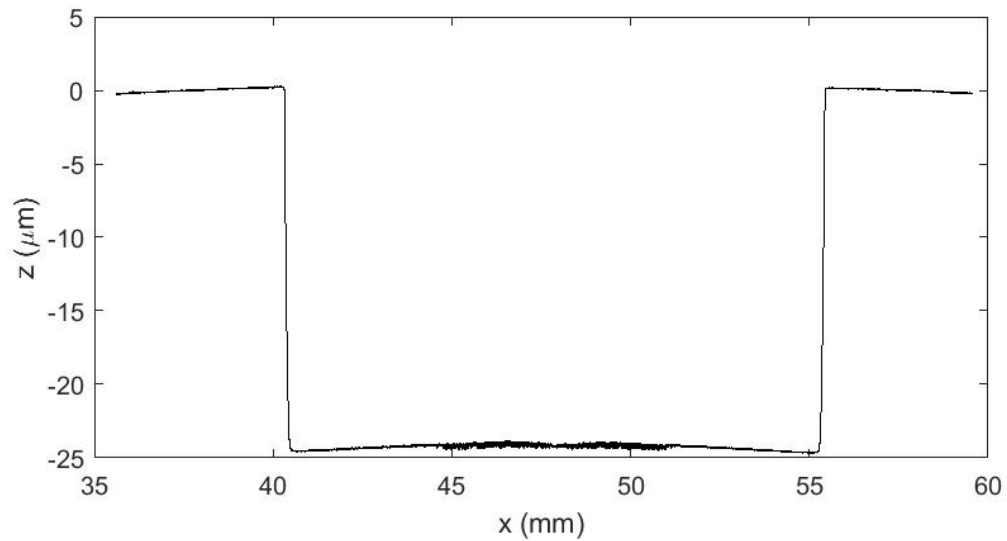


Figure 4.12 Profilometer measurement of the 25  $\mu\text{m}$  PMMA 'top hat' stamper

The spindle on the Precitech was out of square and the stampers had approximately 1.5  $\mu\text{m}$  of cone across 25 mm at the base of the recessed cylinder. The profile measurements were taken to verify the depth of the cylinder as well as to compare the thickness of the replicated cylinder to the stamper. Multiple replications were made for each of the stampers. The 25  $\mu\text{m}$  replications were examined first. Profile measurements of two different replicas are compared to the stamper profile in Figure 4.13.

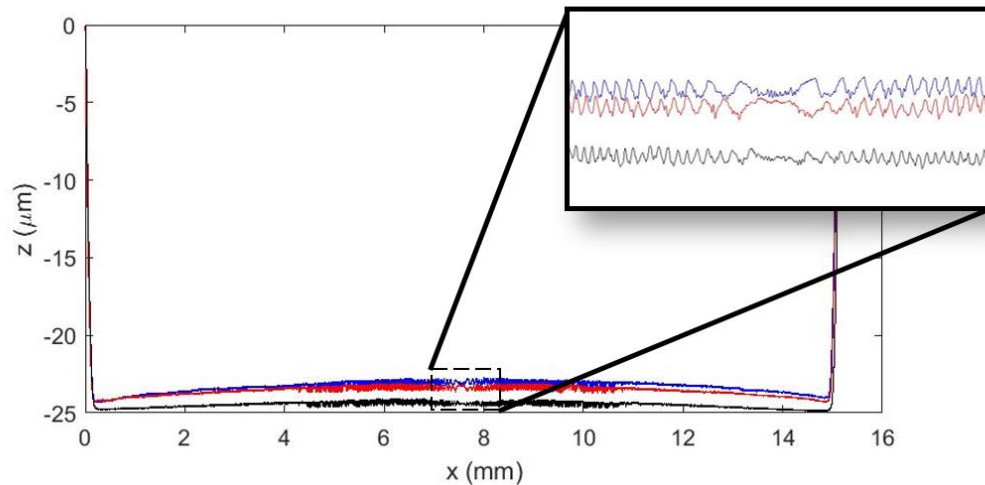


Figure 4.13 Comparison of ‘top hat’ stamper (black) and replications (blue and red)

The profiles of the replicas are shown by the blue and red lines and the stamper can be seen in black. The replicas line up well laterally and are both close to 15 mm in length. The cone in the stamper left a recessed cone in the replicas so the profilometer could be aligned where the stylus was at a minimum in the center of the replication allowing the measurement locations to be centered to  $\pm 5 \mu\text{m}$ . The traces of the replicas and the stamper were aligned at the corner where the cylindrical pillar for the replications and the cylindrical recess for the stamper meet the flange. This plane is considered the neutral plane to examine the shrinkage similar to the sine wave replications made in initial experiments. The center of the measurements shows that the replication process reproduces the fine surface structure of the stamper. The center of the measurement also shows that there is significant shrinkage and that the shrinkage between the two replicas are slightly different. This difference in shrinkage can be explained by examining the full profiles of each replica shown in Figure 4.14.

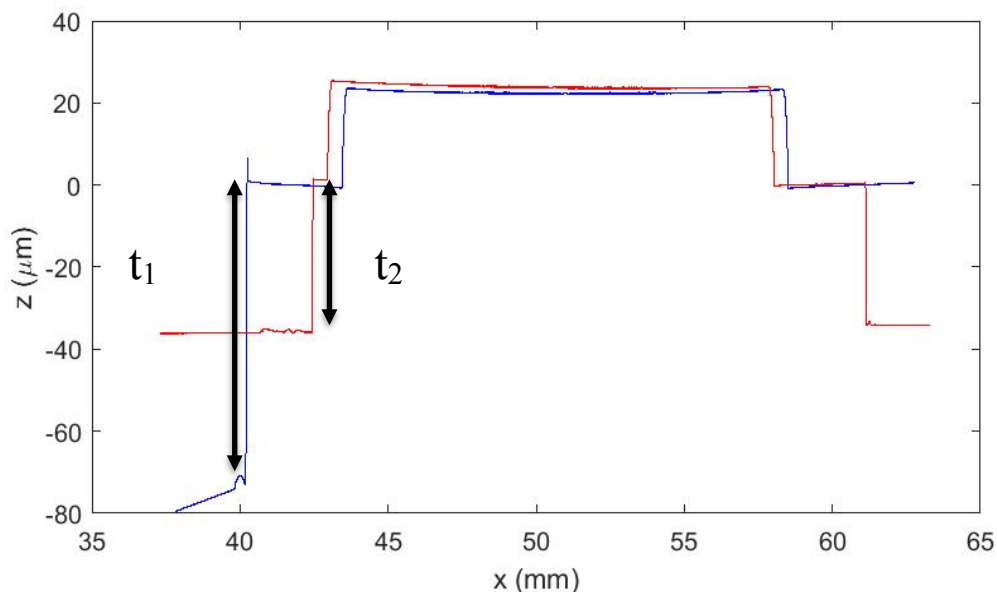


Figure 4.14 Profilometry measurements of different 'top hat' replications

The profile measurements of both replicas show different thickness between the glass substrate and the neutral plane indicated by  $t_1$  and  $t_2$  in Figure 4.14. The difference between  $t_1$  and  $t_2$  is a result of the different thickness of the glass substrates. This difference in thickness results in different total shrinkage. The thickness  $t_1$  corresponds to greater shrinkage in Figure 4.13. The thicker blue replica shrank more than the red replica. This was not the intended result of these experiments; however bulk shrinkage was observed, and further experiments were conducted. The replications system with the split spacer ring, along with the improved substrate holder, allowed for repeatable experiments to be conducted with spheres.

#### 5.4 Spherical Replications

The force measurement experiments showed that PTFE was a suitable stamper material as it resulted in the lowest release force. The cutting experiments showed that it

was difficult to achieve the desired surface roughness in PTFE, however for the shrinkage analysis the high repeatability achieved with the PTFE and overall form obtained with the stamper was advantageous. A spherical PTFE stamper can be seen in

Figure 4.15.

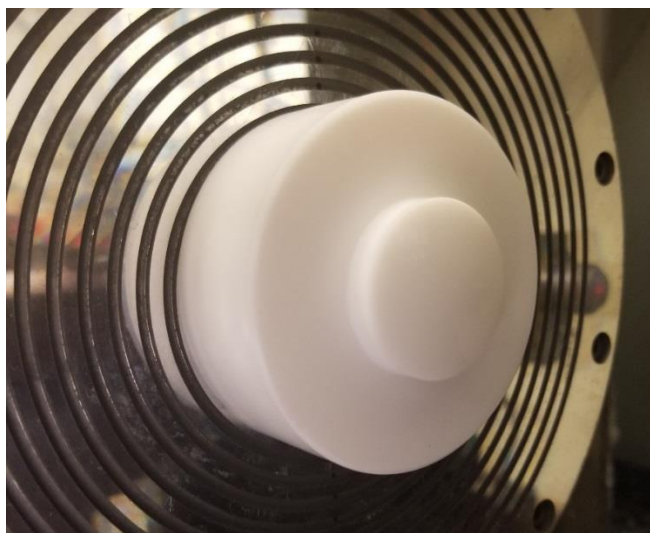


Figure 4.15 Spherical Teflon Stamper

The PTFE stamper was machined on the Moore Nanotechnology 350 FG. This allowed for a tool to be set up to cut the sphere and after verification of the correction term the freeform could then be cut into the PTFE using coordinated axis turning. The spherical replications used the latest replication system with the split spacer ring. This replication system has better repeatability and the same glass substrate was reused for all experiments to reduce uncertainty related to glass substrate thickness variations. The glass substrate has a different radius than the stamper as for the reasons demonstrated in preliminary experiments (see Figure 2.6). The volume of J-91 was held constant for these replication experiments using an auto-pipet dispensing system. The volume for the first

replication tests was 200  $\mu\text{L}$  and the volume for the second set of tests was 400  $\mu\text{L}$ . The repeatability of the auto-pipette volume was measured for 10 experimental dispensations and the standard deviation was found to be less than 0.1% by mass. The volume was increased on the second correction term to evaluate the error in the replication at the edges of the stamper. This increased the replication area. The replications were cured in the ELC-500 for 18 min.

### 5.5 Shrinkage Correction

Profiles of the spherical replicas were made by scan across the glass substrate and up onto the area of the spherical replica. This ensured that the entire optical surface of the replica was captured. An example of a profile of a spherical replica for first set of experiments can be seen in Figure 4.16 below.

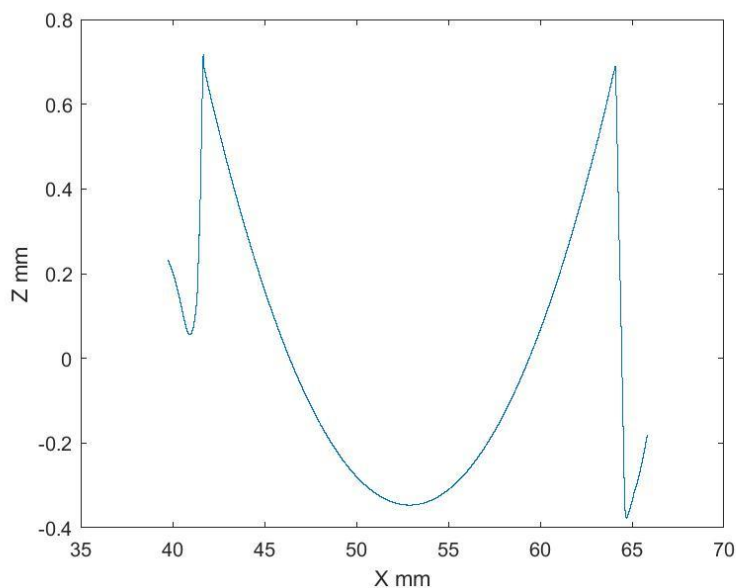


Figure 4.16 Profile of spherical replication

The shrinkage correction term is generated by analyzing the form of the spherical replica using profilometry and comparing it to the stamper. The stamper profile was

measured before the replication process and then the profile of the replication was measured and processed. The spherical replica data was trimmed to compare the spherical surface of the replica to the stamper. Once the profile is trimmed then the difference between the replica profile and the stamper profile to produce the error. This error is then used to correct the shape of the stamper. The major difference between the stamper and the replica is likely due to polymer shrinkage during curing. The shrinkage error term for one replica is shown in

Figure 4.17.

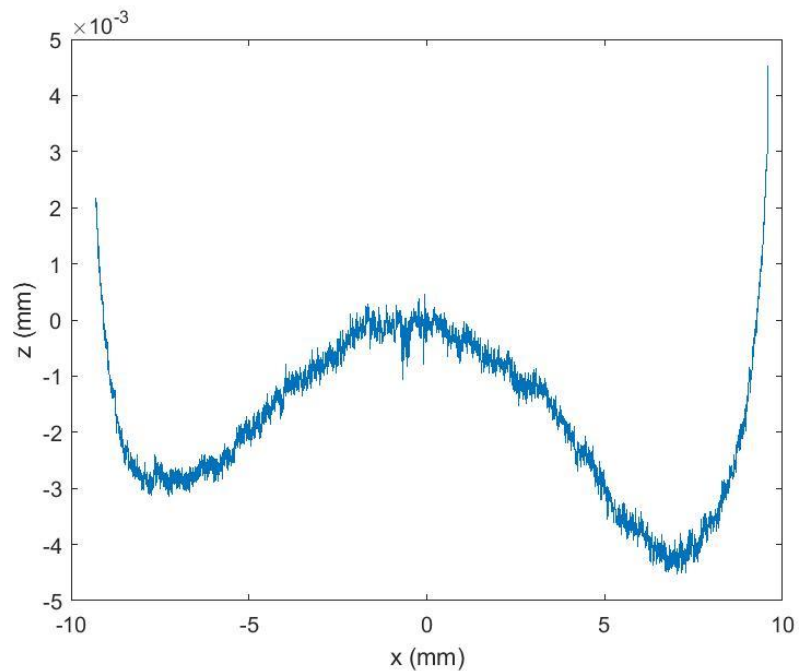


Figure 4.17 Error between stamper and replica – example case

The error was fit with a polynomial to reduce the noise. The polynomial was fit within a 5 mm radius due to the high slope in the error at the edge of the replicas. The area of the replicas was increased on the second iteration of the replications to further

examine the shrinkage near the edge. The polynomial fit to the errors was used as a correction to re-machine the stamper. The polynomial fit can is shown in Figure 4.18.

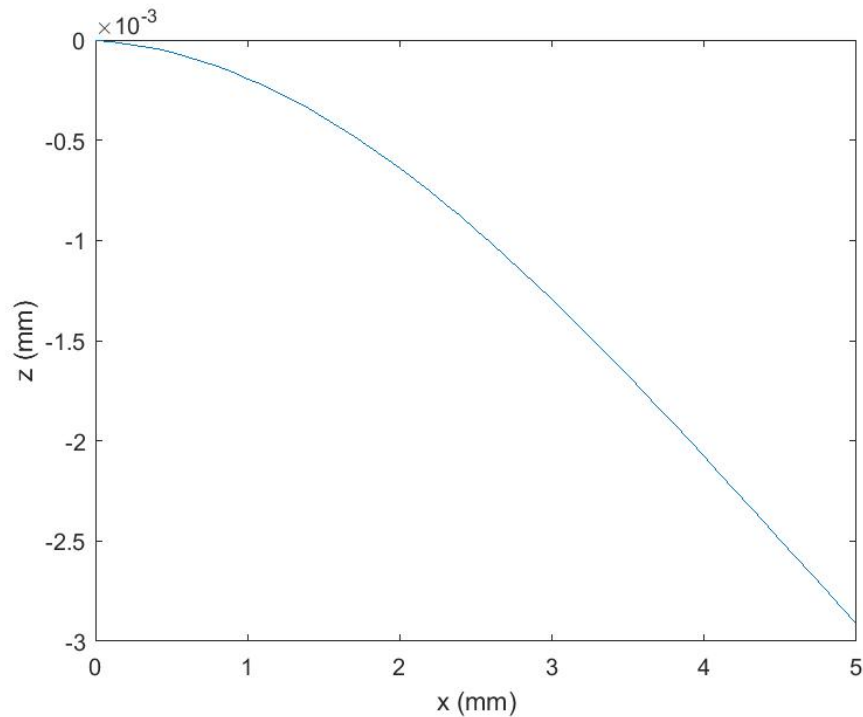


Figure 4.18 Polynomial error fit 5 mm radial region

Once this radial correction term was added to the tool path for the base sphere of the freeform prescription a new Teflon stamper was machined. The base radius is 61.688 mm. The new stamper was used to create four replicas resulting in eight data sets. These data sets were processed in the same way and compared to the prescription of the base radius. This resulted in a new set of error profiles. The new set of profiles is shown in Figure 4.19.

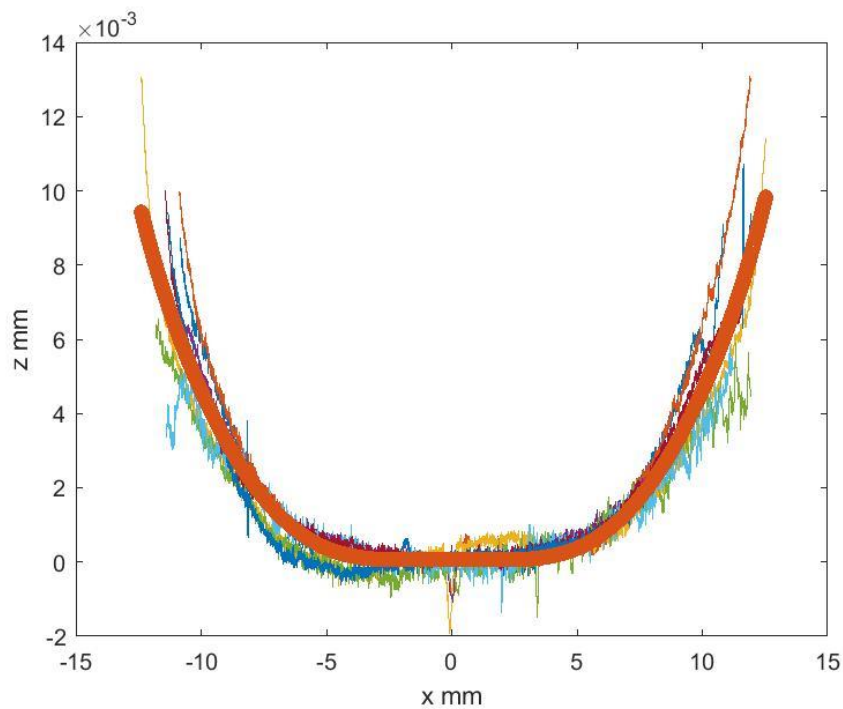


Figure 4.19 Shrinkage error from correct M1 prescription over approximately 27 mm

The profiles of the corrected replications have a lower error in the center 10 mm where the correction was applied. This shows that the shrinkage in the center 10 mm was corrected using the error term generated. There is some residual shrinkage error that will be accounted for in further iterations. This process can be repeated until the error between the replications and the prescription falls below the tolerance value. The error from Figure 4.19 can now be applied again to reduce the errors past the center 10 mm. The comparison between the original shrinkage error and the corrected profile average can be seen in Figure 4.20.

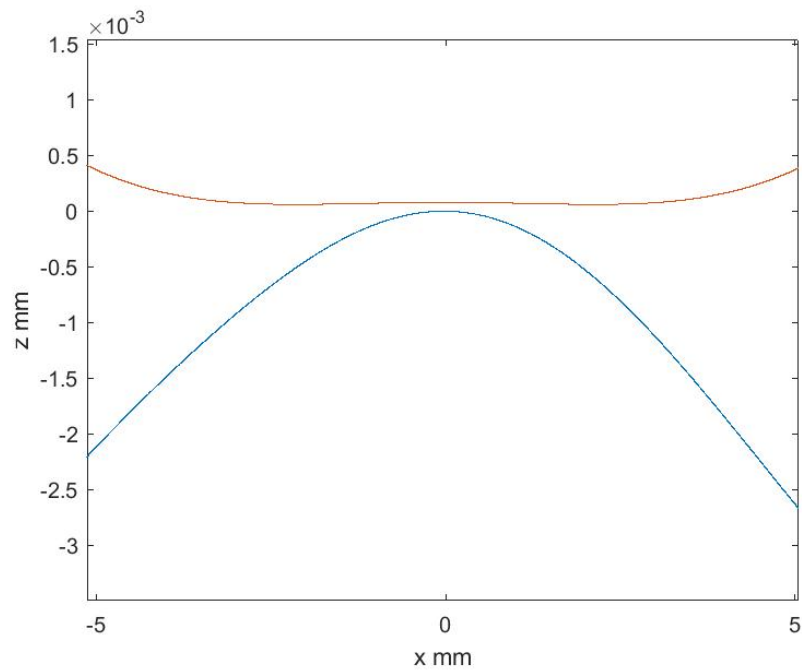


Figure 4.20 Comparison of original error profile (blue) to corrected average (orange)

The shrinkage error in the center 10 mm base sphere for the M1 prescription was reduced from approximately 2.2  $\mu\text{m}$  P-V error to 0.48 P-V with one correction. The average shrinkage error from Figure 4.19 will be applied to the next iteration of the stamper to reduce the error outside the center 10 mm.

## CHAPTER 6: CONCLUSIONS AND FUTURE WORK

### 6.1 Introduction

This chapter serves to cover conclusions and possible future work to be done to further the project. In Chapter 2 the kinematics of the replication process were discussed, and an iterative approach was taken to develop a replication system capable of repeatably producing replications was examined. Different materials were tested in Chapter 3 to determine the optimal material combination to reduce the release force for the replication system. The forces during the release process were measured and examined to help better understand the process. The surface roughness of diamond turned Teflon was examined in Chapter 4. This served as a study to see if the surface roughness of Teflon followed the theoretical roughness as do other diamond turnable materials. The replication process and results are covered in Chapter 5. Shrinkage was observed and corrected for in spherical replications in preparation for freeform replications. Freeform replications were not conducted and will be included in possible future works.

For further improvement of the replication process a variety of UV polymers should be tested to determine the best combination for the application. Material testing should be conducted on electroless nickel with Teflon dispersed within the matrix. This has been seen in standard molding processes to increase mold tool life and to decrease forces during the molding process. The final replication system should be tested to quantify repeatability and positional accuracy of the system.

## REFERENCES

- [1] K. P. Thompson and J. P. Rolland, "Freeform Optical Surfaces: A Revolution in Imaging Optical Design," *Opt. Photonics News*, vol. 23, no. 6, pp. 30–35, 2012.
- [2] E. Abbe, "Lens system." Google Patents, 22-Apr-1902.
- [3] C. J. Evans, "Precision engineering: An evolutionary perspective," *Philos. Trans. R. Soc. A Math. Phys. Eng. Sci.*, vol. 370, no. 1973, pp. 3835–3851, 2012.
- [4] F. Z. Fang, X. D. Zhang, A. Weckenmann, G. X. Zhang, and C. Evans, "Manufacturing and measurement of freeform optics," *CIRP Ann. - Manuf. Technol.*, vol. 62, no. 2, pp. 823–846, 2013.
- [5] J. Ye, L. Chen, X. Li, Q. Yuan, and Z. Gao, "Review of optical freeform surface representation technique and its application," *Opt. Eng.*, vol. 56, no. 11, p. 1, 2017.
- [6] D. C. Thompson, "<title>Theoretical Tool Movement Required To Diamond Turn An Off-Axis Paraboloid On Axis</title>," *Adv. Precis. Mach. Opt.*, vol. 0093, no. December 1976, pp. 23–31, 2012.
- [7] S. Douglas, "A Machining System for Turning Nonaxisymmetric Surfaces," 1983.
- [8] L. W. Alvarez, "Two-element variable-power spherical lens." Google Patents, 21-Feb-1967.
- [9] B. S. Dutterer *et al.*, "Diamond milling of an Alvarez lens in germanium," *Precis. Eng.*, vol. 38, no. 2, pp. 398–408, 2014.
- [10] J. D. Owen, J. A. Shultz, T. J. Suleski, and M. A. Davies, "Error correction methodology for ultra-precision three-axis milling of freeform optics," *CIRP Ann. - Manuf. Technol.*, vol. 66, no. 1, pp. 97–100, 2017.
- [11] H. Karow, *Fabrication methods for precision optics*. Hoboken: Wiley-Interscience, 2004.
- [12] G. C. Firestone, A. Jain, and A. Y. Yi, "Precision laboratory apparatus for high temperature compression molding of glass lenses," *Rev. Sci. Instrum.*, vol. 76, no. 6, 2005.
- [13] K. D. Fischbach *et al.*, "Investigation of the effects of process parameters on the glass-to-mold sticking force during precision glass molding," *Surf. Coatings Technol.*, vol. 205, no. 2, pp. 312–319, 2010.
- [14] P. Wachtel, P. Mosaddegh, B. Gleason, J. D. Musgraves, and K. Richardson, "Performance evaluation of a bench-top precision glass molding machine," *Adv.*

*Mech. Eng.*, vol. 2013, 2013.

- [15] P. Mosaddegh and J. C. Ziegert, "Friction measurement in precision glass molding: An experimental study," *J. Non. Cryst. Solids*, vol. 357, no. 16–17, pp. 3221–3225, 2011.
- [16] F. Klocke, K. Georgiadis, O. Dambon, K.-D. Bouzakis, S. Gerardis, and G. Skordaris, "A complete qualification methodology for coatings of precision glass molding tools," *Opt. Manuf. Test. IX*, vol. 8126, no. September 2011, p. 81260T, 2011.
- [17] P. He *et al.*, "Graphene-coated Si mold for precision glass optics molding," *Opt. Lett.*, vol. 38, no. 14, p. 2625, 2013.
- [18] F. Bernhardt, K. Georgiadis, L. Dolle, O. Dambon, and F. Klocke, "Development of a ta-C diamond-like carbon (DLC) coating by magnetron sputtering for use in precision glass molding," *Materwiss. Werksstech.*, vol. 44, no. 8, pp. 661–666, 2013.
- [19] A. Symmons and B. Auz, "Design considerations and manufacturing limitations of Insert Precision Glass Molding (IPGM)," *Polym. Opt. Molded Glas. Opt. Des. Fabr. Mater. II*, vol. 8489, no. October 2012, p. 84890H, 2013.
- [20] A. Symmons, J. Huddleston, and D. Knowles, "Design for manufacturability and optical performance trade-offs using precision glass molded aspheric lenses," *Polym. Opt. Molded Glas. Opt. Des. Fabr. Mater. 2016*, vol. 9949, no. September 2016, p. 994909, 2016.
- [21] D. Gurganus, J. D. Owen, M. A. Davies, B. S. Dutterer, S. Novak, and A. Symmons, "Precision glass molding of freeform optics," no. September 2018, p. 28, 2018.
- [22] L. Su, F. Wang, P. He, O. Dambon, F. Klocke, and A. Y. Yi, "An integrated solution for mold shape modification in precision glass molding to compensate refractive index change and geometric deviation," *Opt. Lasers Eng.*, vol. 53, pp. 98–103, 2014.
- [23] D. J. Resnick and J. Choi, "A review of nanoimprint lithography for high-volume semiconductor device manufacturing," *Adv. Opt. Technol.*, vol. 6, no. 3–4, pp. 229–241, 2017.
- [24] D. C. O'Shea, T. J. Suleski, A. D. Kathman, and D. W. Prather, "Survey of Fabrication Techniques for Diffractive Optical Elements," *Diffractive Opt.*, pp. 149–166, 2009.

- [25] Stephen D. Fantone, "Replicating Optical Surfaces Using UV Curing Cements: A Method," *Appl. Opt.*, vol. 22, no. 6, p. 1983, 1983.
- [26] R. J. M. Zwiars and G. C. M. Dortant, "Aspherical lenses produced by a fast high-precision replication process using UV-curable coatings," *Appl. Opt.*, vol. 24, no. 24, p. 4483, 2009.
- [27] T. Bifano, TG Dow and R. Scattergood, "Ductile-regime Grinding - A New Technology For Machining Brittle Materials," *J. Eng. Ind. Asme*, vol. 113, no. 2, pp. 184–189, 1991.
- [28] D. Ravindra and J. Patten, "Ductile regime single point diamond turning of quartz resulting in an improved and damage-free surface," *Mach. Sci. Technol.*, vol. 15, no. 4, pp. 357–375, 2011.
- [29] J. M. Tamkin and T. D. Milster, "Effects of structured mid-spatial frequency surface errors on image performance," *Appl. Opt.*, vol. 49, no. 33, p. 6522, 2010.
- [30] J. Reimers, A. Bauer, K. P. Thompson, and J. P. Rolland, "Freeform spectrometer enabling increased compactness," *Light Sci. Appl.*, vol. 6, no. 7, p. e17026, 2017.
- [31] F. Awaja, M. Gilbert, G. Kelly, B. Fox, and P. J. Pigram, "Adhesion of polymers," *Prog. Polym. Sci.*, vol. 34, no. 9, pp. 948–968, 2009.
- [32] E. Paul, C. J. Evans, A. Mangamelli, M. L. McGlaufflin, and R. S. Polvani, "Chemical aspects of tool wear in single point diamond turning," *Precis. Eng.*, vol. 18, no. 1, pp. 4–19, 1996.
- [33] E. L. Church and J. M. Zavada, "Residual surface roughness of diamond-turned optics," *Appl. Opt.*, vol. 14, no. 8, p. 1788, 2008.
- [34] J. Qu and A. J. Shih, "Analytical surface roughness parameters of a theoretical profile consisting of elliptical arcs," *Mach. Sci. Technol.*, vol. 7, no. 2, pp. 281–294, 2003.
- [35] J. W. Carr and C. Feger, "Ultraprecision machining of polymers," *Precis. Eng.*, vol. 15, no. 4, pp. 221–237, 1993.
- [36] Y. C. Cheng, P. J. Wang, and W. Y. Hsu, "Investigation of Characteristics of Ni-P-PTFE Coating on Optical Molds," *Mater. Sci. Forum*, vol. 773–774, pp. 697–704, 2013.

- [37] A. Sohn and T. A. Dow, "Removal of Form Error in Replicated Optics," *ASPE Spring Top. Meet. Precis. Fabr. Replication*, vol. 19, 1999.
- [38] C. Ochoa-Putman and U. K. Vaidya, "Mechanisms of interfacial adhesion in metal-polymer composites - Effect of chemical treatment," *Compos. Part A Appl. Sci. Manuf.*, vol. 42, no. 8, pp. 906–915, 2011.